AN ABSTRACT OF THE THESIS OF

Matthew H. Kremer for the degree of Master of Science in Materials Science presented on June 5, 2019.

Title: Electrospray Deposition of Discrete Nanoparticles: Studies on Pulsed-Field Electrospray and Analytical Applications

Abstract approved: _____

Vincent T. Remcho

Electrospinning and electrospray are both nano-scale material fabrication techniques, based on related phenomena of electrically charged fluid spray from a droplet of liquid. Material is dissolved in liquid, then a spray is generated by applying a high voltage, creating an electric field, between the fluid dispensing capillary and a grounded collection substrate. Nano-scale features of the dissolved material are collected when the solvent evaporates in flight between the needle and collection substrate. Though electrospinning and electrospray are terms that can be used interchangeably (they frequently are) electrospinning specifically refers to using the technique to generate nanofibers; electrospray is a more appropriate term for the spray of individual, charged droplets. Electrospray theory is also seen applied in electrospray ionization interfaces to mass spectrometers. The underlying principles of electrospray for mass spectrometry and electrospray for deposition are the same, but deposition targets a bulk coating of material instead of quantitative analysis of a small number of gas phase analytes. In this work, electrospray deposition of discrete features from individual, charged droplets was realized.

There is some literature published on this topic, but electrospinning literature is overwhelmingly populated with work on the fabrication of continuous nanofibers and "beaded features" are typically considered as defects in desired morphologies.

A significant portion of this work was in collaboration on a DARPA funded research project with a local industry sponsor. Due to compliance with non-disclosure, the exact motivation and specific applications to that project cannot be discussed in this thesis, although the premise can be addressed. The broad goal of the project was development of techniques and methodology for assembling structures comprising features spanning nano, micro and macro scale dimensions. On that project, electrospray was used to fabricate discrete nanoplate features on the order of 100-200nm in size. These features were deposited, using the electrospray technique, onto a branched architecture with dimensions on the micron length scale. Effort went toward controlling the size of these features through electrospray parameters and demonstrating the repeatability in deposition of these features onto the device architecture.

Outside of the sponsored project work, generation of discrete nano-plate/particle features from protein and polymer materials was used in both direct applications and to investigate the impact of pulsed high voltage (or pulsed-field) on the electrospray process. The technique was used directly in two analytical chemistry applications: first, the deposition of blood coagulation chemistries onto a point-of-care-applicable blood plasma separation device, with the goal of improving its separative performance; and second, electrospray deposition of an enzyme on the working electrode in an electrochemical sensor application for glucose detection.

Design, fabrication, and implementation of custom components was done using 3D printing, laser cutting, and CNC end-milling to facilitate both research toward the sponsored project and work discussed in this thesis. An acrylic enclosure was used for the depositions and saw several modifications to meet changing research needs. To study pulsed-field electrospray a transformer-based high voltage system was designed and assembled in-lab. This system had limitations but was applicable for generating high voltage pulse waveforms and was used to perform electrospray deposition research.

Electrospray Deposition of Discrete Nanoparticles: Studies on Pulsed-Field Electrospray and Analytical Applications

by
Matthew H. Kremer

A THESIS

submitted to

Oregon State University

in partial fulfillment of
the requirements for the
degree of

Master of Science

Presented June 5, 2019
Commencement June 2019

Master of Science thesis of Matthew H. Kremer presented on June 5, 2019

APPROVED:

Major Professor, representing Materials Science

Director of the Materials Science Program

Dean of the Graduate School

I understand that my thesis will become part of the permanent collection of Oregon State University libraries. My signature below authorizes release of my thesis to any reader upon request.

Matthew H. Kremer, Author

ACKNOWLEDGEMENTS

I must first and foremost acknowledge my advisor, Dr. Vincent Remcho, whose support, encouragement, and mentorship has shaped me both professionally and personally. I have no doubt that the skills I have developed during my time here will serve me going forward.

I received tremendous support, guidance, and knowledge from all members of the Remcho Research Group and from those who spent time in the lab, especially Dr. Christopher Heist, Dr. Sumate Pengpumkiat, Andrew McKelvey, Dr. Chandima Bandara, Nadeeshani Jayathilake, Owen Shellhammer, Lindsay Unitan, David Bemis, Rylie Tiffin, Andrew Berghorn, Siraprapa (Fern) Boobphahom, Michelle Tran, Saichon Sumantakul, and Chadd Armstrong. You were my collaborators, commiserators, and I will always call you my friends. My graduate research experience and my life have been profoundly impacted by you.

I owe much thanks to Mark Warner, formerly of the Oregon State University Chemistry Department Electronics Shop, he helped me significantly in developing and implementing the first transformer-based pulsed high voltage system that we used in the beginning of this research. Thank you to Dr. Shay Bracha, for his assistance in obtaining biological samples. Thank you to Pete Eschbach and Teresa Sawyer of the OSU Electron Microscopy Facility for training and assistance performing electron microscopy.

My position as a graduate research assistant was supported by Voxtel Inc. on a project funded by DARPA. Their support for my position and collaboration was essential. Thank you especially to Paul Harmon, Ngoc Nguyen, Kory Plakos and Sean Keuleyan.

CONTRIBUTION OF AUTHORS

I began work on this project with Andrew McKelvey, though the only evidence of his work in this thesis is toward the electrospray enclosure and the keratin/PEO solution preparation; he set up the first electrospray apparatuses and conducted experiments and optimizations that began this research project. His contributions cannot go unrecognized. Dr. Chandima Bandara assisted in collection of data for Chapter 3 and provided the device technology he developed for use in collaboration on those experiments. Lindsay Unitan assisted in device fabrication for experiments. Nadeeshani Jayathilake assisted on the work in Chapter 4 by collection and interpretation of electrochemical sensor data and sharing her knowledge and expertise on electrochemical detection. Both Nadeeshani and Chandima assisted in design of experiments for the electrochemical sensor work.

TABLE OF CONTENTS

Page

TABLE OF CONTENTS (Continued)

Page

TABLE OF CONTENTS (Continued)

Page

LIST OF FIGURES

Figure Page

LIST OF FIGURES (Continued)

Figure Page

LIST OF FIGURES (Continued)

Figure Page

LIST OF APPENDIX FIGURES

Figure Page

LIST OF APPENDIX TABLES

Table Page

DEDICATION

To my loving and supportive family:
my father, William Kremer;
my mother, Debra Kremer;
my brother, Samuel Kremer.
You are the foundation which has allowed me to keep going throughout the pursuit of my education.

To my grandmother, LaVerta Lammers, may I strive to achieve the selflessness and care which you share in the service of others.

Chapter 1: Introduction

1.1 Electrospinning history

Electrospinning is a relatively old technique. The first studies into the behavior of electrically charged fluids date to as early as 1600[1]. Though, this is not actually electrospinning, merely observations of fluid behavior in the presence of charged objects and that a spray of smaller droplets can be created from a droplet of liquid. The first journal publication by John Zeleny[2] on electrospinning details a setup comparable to contemporary research setups and dates to 1914. In 1930, Anton Formhals began a series of patents on the technique for electrospinning of fibers[3]. In the 1960s Geoffrey Taylor published mathematical studies of the cone formation at the tip of the charged droplet[4]. This cone phenomenon bears his name as the "Taylor cone" and is a distinct aspect of the electrospinning process. In the 1990s, researchers lead significant advancements to the understanding of the electrospinning process in publications on fabrication of nanofibers from polymer materials. Notable contributions during that time come from D.H. Reneker's group, who popularized the term "electrospinning" to apply to the technique[5].

1.2 Methodology and general applications

Electrospinning is used to fabricate micro or nanoscale dimensional fibers from a variety of materials (polymer[6], biological materials/proteins[7], metals[8]) dissolved in solution. Electrospinning of continuous nanoscale fibers is achieved when sufficiently high voltage is applied to a droplet of liquid, overcoming the surface tension forces on the droplet and causing electrostatic repulsion of a jet of solution outward from the droplet[9].

Applications have been reported employing the technique for fabrication of bulk, fibrous, non-woven nanomaterials[10-12]; electrospinning has also been used to craft filtration membranes having controlled pore size, by controlling the features of the deposited fiber network[13,14]. Incorporation of bioproteins with polymer materials has seen application in electrospun wound dressings, with the goal to accelerate the healing process of open wounds[15,16]. Electrospun nanofibers have been functionalized and employed for sensor applications, which they lend themselves well to, due to having a high surface area to volume ratio[17–21]. Functionalization is usually achieved either by incorporation of a functional material into the polymer electrospinning solution or by surface functionalization of the electrospun material after deposition. Electrospinning of functional sensing materials as nanofibers has also been demonstrated[22–26], either as an electrochemical or impedance sensor. Additionally, electrospinning of biological protein (natural polymer) systems has been applied to fabrication of wound dressing materials, fibrous networks which mimic the extra-cellular matrix, and for drug delivery and tissue engineering studies[7,15,27–30].

1.3 Applications in this research

Electrospinning and electrospray are related processes and the terms are often used interchangeably, however they describe different behavior and different morphologies of generated material. Fiber electrospinning parameters can be tuned so that continuous fibers are no longer formed, which defines the region between electrospinning of continuous nanofibers and electrospray of discrete morphologies. In this work, deposition of discrete

morphologies was achieved and used for the study of pulsed DC voltage impact on the deposition process. The enzyme glucose oxidase was incorporated in an aqueous solution with glutaraldehyde and electrosprayed for an enzymatic glucose sensor application. The proteins fibrinogen, keratin and bovine serum albumin were electrosprayed to create discrete biological nanofeatures. Since fibrinogen plays a key role in blood clot formation, as a component of the blood coagulation cascade, we were also inspired to study its application for enhancing the performance of a microfluidic blood plasma separation device through surface modification with the coagulating chemistry.

1.4 Electrospinning setup

There are three main components required for the electrospinning setup: a high voltage power supply, a syringe pump, and an enclosure for mounting components of the apparatus. The high voltage power supply is used to supply the high potential which drives the electrospinning processes by generation of an electric field. The syringe pump is used to dispense the electrospinning solution from a needle or capillary at a controlled rate. Most research electrospinning setups are assembled in-lab to meet the specific needs of the researcher. Though, there are several commercially produced setups available from companies specifically offering systems for industrial production[31] but there are also companies offering both industrial and laboratory/R&D setups[32–35]. The high voltage power supply and syringe pump components of the electrospinning setup are usually commercial systems and are not something developed in-house, except in certain circumstances (such as the pulsed high voltage system in this work). The enclosure

component of the setup, where the needle and collection target are mounted, is frequently a component that is devised and assembled by the researcher to meet their specific needs.

For our initial setup, we modified an acrylic boxing glove display case to serve as the deposition chamber, shown in Figure 1.1. It was set up so that it was enclosed from but not sealed from the outside environment. The needle was fed through a hole/inlet in the side of the chamber, which positioned it co-axial with the center of a metal post. The metal mounting post was secured into an acrylic holder plate which could be removed from the chamber to facilitate ease of sample mounting and removal. The mounting post holder was attached to a linear adjustment screw mounted inside of the electrospinning enclosure. This linear motion attachment allowed for manual adjustment of distance between the spray needle tip and the collector substrate's surface (i.e. the separation/deposition distance). In

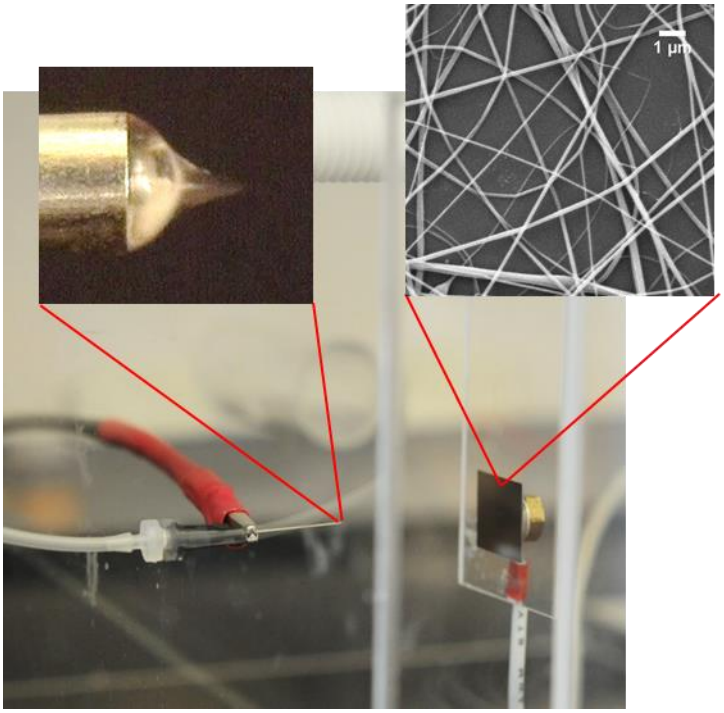

Figure 1.1: Electrospinning setup showing spray source (with high voltage supply connected) and a silicon substrate mounted on grounding post. Cut-away images show enlarged version of spray cone and example image of electrospun fibers.

our setup the orientation of the syringe and needle were horizontal. The needle entered the side wall of the chamber, so spray was generated in a horizontal direction and collected on substrates mounted orthogonal to the work surface. This is opposed to a vertical orientation, where the spray needle enters the chamber through the top wall and the substrate is mounted below the needle. Both horizontal[5] and vertical[6] setups are reported. Few have studied the differences between the two in term of resulting morphologies[36]. We found the vertical orientation to be a potential shock hazard on disassembly or removal of the needle due to the potential of conductive liquids to leak from the syringe and maintain a charge.

1.5 Electrospray vs electrospinning

1.5.1 Morphology continuum: beads to fibers

Electrospray encompasses the regime of electrospinning where fibers are not created, and instead discrete nano to microscale features, or "beads", of material are deposited. These discrete materials can be achieved with polymer materials by reducing the concentration of polymer in the electrospray solution below a critical level. The relationship between increasing polymer concentration and resulting morphologies is listed by Shenoy et al.: beads, beaded fibers, fibers only, and globular fibers with macrobeads[37]. An example of steps on this continuum in electrospray morphology due to polymer concentration is shown from our own results in Figure 1.2. The deposited nanofibers shown here are a protein/polymer blend of keratin/PEO in the solvent trifluoroethanol (TFE) prepared using a reported method[38]. The ratio of protein to

polymer in solution was 9:1. In this case, fiber morphology was seen from depositions of the 20 mg/mL keratin/PEO in TFE solution. Although, there is some bead-in-fiber formation and they are not perfectly continuous diameter nanofibers. When the 10 mg/mL solution is electrospun the morphology is distinctly different, as there is clearly no fiber formation and only discontinuous, discrete nano-to-micro-scale particles. We were primarily interested in the electrospinning (or electrospray) of discrete bead features, because this morphology was considered to be more conducive to study of orientation effects due to changes in parameters.

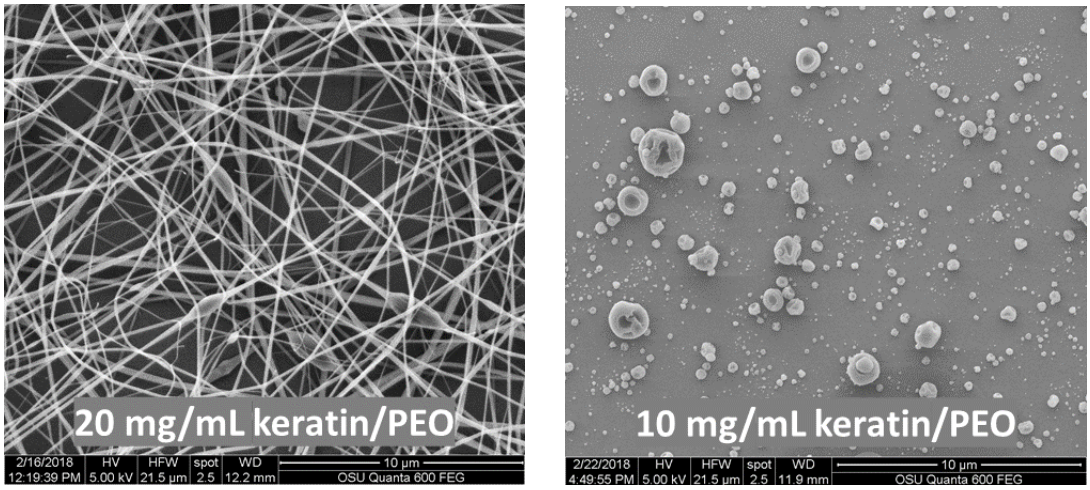

Figure 1.2: Electrospinning of 9:1 keratin:PEO in TFE demonstrating continuous fibers (left) and discontinuous discrete features (right).

1.5.2 Electrospray of discrete particles

When operating in the discrete particle spray mode of electrospinning, it is likely that the process follows the model of electrospray ionization (ESI), shown in the left panel of Fig. 1.3. Models for electrospray ionization have been developed for application in mass spectrometry. In the charge residue model of ESI theory, droplets are generated from the

Taylor cone when a sufficient voltage is applied to overcome the surface tension of the droplet[39]. The first generation of droplets undergo droplet shrinkage due to evaporation while en-route to the collector substrate (for mass spectrometry, this would be the skimmer/inlet)[39]. The droplet volume decreases such that the charge on the droplet causes further cone formation and droplet ejection into another generation of charged droplets; this process continues into multple generations, creating subsequently smaller droplets[39]. The charge residue model (right panel of Fig. 1.3) is applied to large globular proteins[40]. Through this process, the final product is an evaporated droplet where only the material contained in the original droplet remains. The charge from the droplet is transferred to the material and the particle is collected on the grounded substrate.

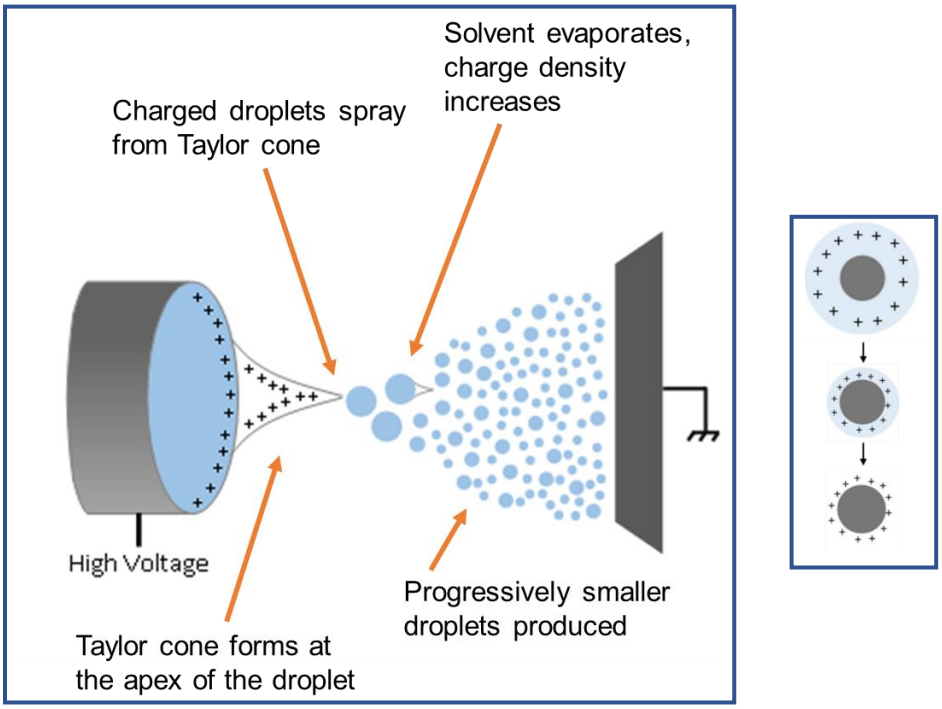

Figure 1.3: (Left) Depiction of electrospray and Taylor cone formation on tip of capillary. **(Right)** Charge reside model of electrospray ionization theory.

1.6 Key electrospinning parameters

The electrospinning or electrospray process is dependent on a relatively large parameter set. The range of many of these parameters is enough that variation outside of an ideal range may lead to either subtle or significant variations in the results or may result in no electrospray generation at all. The parameters are interdependent, what is appropriate in one scenario may not apply in others, due to variation of one parameter impacting the appropriate range of another. These parameters are namely: applied voltage, needle to collector (counter-electrode) distance, solution flow rate, solvent (or multi-solvent system), inner and outer diameter of dispensing needle or capillary, electrospray material, material concentration in solution, collector substrate geometry, and atmosphere conditions. These parameters and their impact on the electrospray process will be described in more detail in the following sections. Typical values for these ranges, from reports in literature, will be contrasted with ranges from this work.

1.6.1 Voltage

The electrospray voltage is a critical parameter in the electrospray process. It is essential for driving the electrospray generation of charged droplets. The voltage required for electrospray generation is dependent on both physical parameters of the electrospray setup, as well as aspects of the solution/material being electrosprayed. Models developed for electrospray ionization (ESI) have detailed an equation to describe the electric field, E_c, required for electrospray generation and the relevant parameters[41]:

$$E_C = 2V_C/[r_C \ln(4d/r_C)] \quad (1.1)$$

Where V_c is the applied voltage, r_c is the outer radius of the capillary and d is the distance from the tip to the grounded electrode. Typically E_c is on the order of 10^6 V/m.[41] Generally, the model underestimated the necessary voltage for specific situations in this research, when assuming an electric field on the order of 10^6 V/m. But, the model is intended for ESI for mass spectrometry of small ionic compounds, not bulk deposition of material. Even if the model is not directly applicable, it still indicates the geometric parameters in the equation are important in the process since they influence the electric field, independent of the voltage applied. It also serves to address the point that the most commonly reported process parameters in electrospinning literature are working voltage and distance from needle to collector. However, it's likely that the electric field varies between different researchers' setups and electrode geometries, so direct replication from reported literature, based solely on voltage and distance parameters, may not give the same results.

Many reports on electrospinning and electrospray use working voltages in the 10kV to 20kV range and some report up to 30kV[6,42,43]. In this work, the range used was almost exclusively below 10kV and typically in the range from 4kV to 9kV. This was largely due to limitations in the high voltage power supply used, because the lab-built, transformer-based pulse system was not capable of supplying voltages greater than ~8kV. Although, because of this limitation, we also saw that electrospray in this lower voltage range is easily practicable. The voltage parameter is interdependent with the needle to collector distance, so this distance had to be reduced accordingly. Those reporting use of higher voltages for electrospinning also use greater distances, in the range of 10 to 20cm,

whereas in this work comparatively lower ranges were used (2 to 5cm). Considered as field strengths (voltage to distance), the typical range of values is 1.5-2.5 kV/cm. Shin et al. showed the effect on Taylor cone behavior due to variation in the applied voltage (expressed at a field strength of kV/cm)[44]. They studied electrospinning with an aqueous PEO solution and saw cone collapse or disappearance at a field strength of 1kV/cm. Generally, we operated in a kV/cm range greater than the maximum working range they reported. However, it is likely that the working range of voltage to distance relationships is also dependent on other factors, such as material and solution parameters.

1.6.2 Needle to collector distance

As mentioned above, applied voltage and needle to collector distance are interrelated parameters. We observed that variation of voltage at a fixed distance covers a range of electrospray behavior. If the applied voltage is too low for a given distance, then no droplet spray generation occurs. This is because the strength of the electric field is too low. Within the working range of voltages at a given distance, a stable Taylor cone is formed and spray is generated. At too high of voltages, for a given distance, spray behavior becomes unstable and multiple jets of spray can be generated, instead of a single, stable cone/jet. Aside from the interrelationship with applied voltage, the collector distance also impacts the deposition behavior. At too close a distance, sprayed droplets (or fibers) may be collected without full evaporation of solvent during the spray process. This results in a different morphology than if the collector were located at a further distance. Determination of whether a distance is “too close” is related to solvents used in the preparation of the

electrospray solution. Aqueous-based solvent systems will be slower to evaporate than organic-based solvent systems at shorter needle-to-collector distances. Electrospray deposition on a flat collector substrate, oriented orthogonally to the spray source, will generally result as a rounded spray area with a gradient of deposition density which decreases from the center toward the outer edge. The width of this spray area generally varied with deposition distance. A shorter distance resulted in smaller more dense spray regions, whereas using a greater distance resulted in a broader deposition area.

1.6.3 Solution flow rate

Within this work, the flow rate to dispense the solution was determined experimentally. If too slow a flow rate the cone shape could collapse and would not give a stable Taylor cone or electrospray behavior. If too fast a flow rate, spray behavior would enter a strong jet mode or would oscillate between a stable cone and droplet projection – neither of which were desirable for spray of discrete features. When large droplets are projected it seems likely that they are unable to evaporate in the space between the needle and collector because the appearance of liquid buildup tends to form on the collector. This is detrimental for the purpose of electrospray deposition, especially considering we noted a significant difference in morphology between electrospray deposited and drop-cast (dispensed in liquid phase) as shown in Figure 1.4. Large droplets that are projected from the Taylor cone during electrospray were observed to cause drop-cast-like features on the collector substrate. Reported working ranges of the flow rate used in electrospinning of

nanofibers are typically 100 to 1000 µL/min[6]. We typically worked in the range of 10-100 µL/hr.

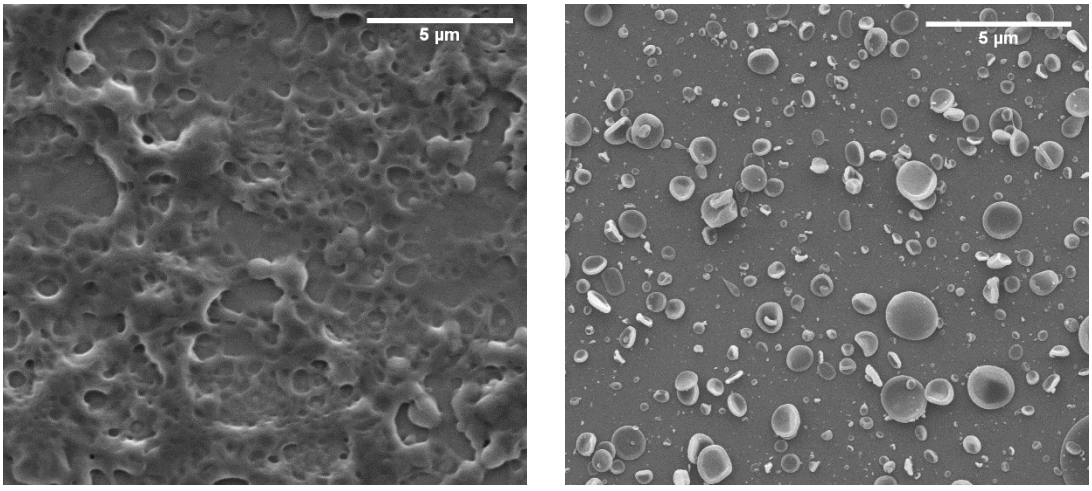

Figure 1.4: Comparison of drop-cast dispensing of electrospinning solution **(Left)** with electrospray deposited results from same solution **(Right)**.

1.6.4 Material concentration in solution

As shown earlier in Fig. 1.2, with electrospray deposition of keratin, material concentration in the electrospinning solution can affect the result on the bead to fiber continuum. Reports have shown that variation of the concentration of material in solution can affect the results for fiber formation[45,46]. There are apparently no reports studying controlled electrospray of beaded features and none known to directly study the material concentration effect on the bead morphology and size distribution. Dong et al. studied electrospray of aqueous wheat gluten solutions which generated similar morphologies to the features seen in our research[42]. Though they evaluated several sources of wheat gluten, they did not conduct comparable experiments between these sources and did not compare varying concentrations from the same source. From our own experience, there is a narrow range of material concentrations in which bead features are created and attempting

to determine the extent of this range did not generate useful results. Instead, effort was put into study of how other electrospray parameters impact the results at a given concentration of material which generated bead features. In this work the primary range of concentrations used was 2mg/ml to 20 mg/ml. In literature on electrospinning of fibers it is much more common to see concentration ranges in the 100s of mg/ml[37], however there are certainly relevant reports of concentrations in comparable ranges to this work.[5,45].

1.6.5 Collector geometry

Interesting behavior was observed in comparison of electrospun fibers onto substrates with patterned morphologies vs planar substrates. Specifically, the deposition of nanofibers from polycaprolactone (Perstorp Capa 6800, 80kDa molecular weight), here prepared as 10 mg/mL in hexafluoro-2-propanol (diluted from 80 mg/mL in chloroform.) Shown in Figure 1.5 is the resulting morphology for deposition under the same conditions, but onto different substrate geometries. The left image is deposition onto a planar silicon

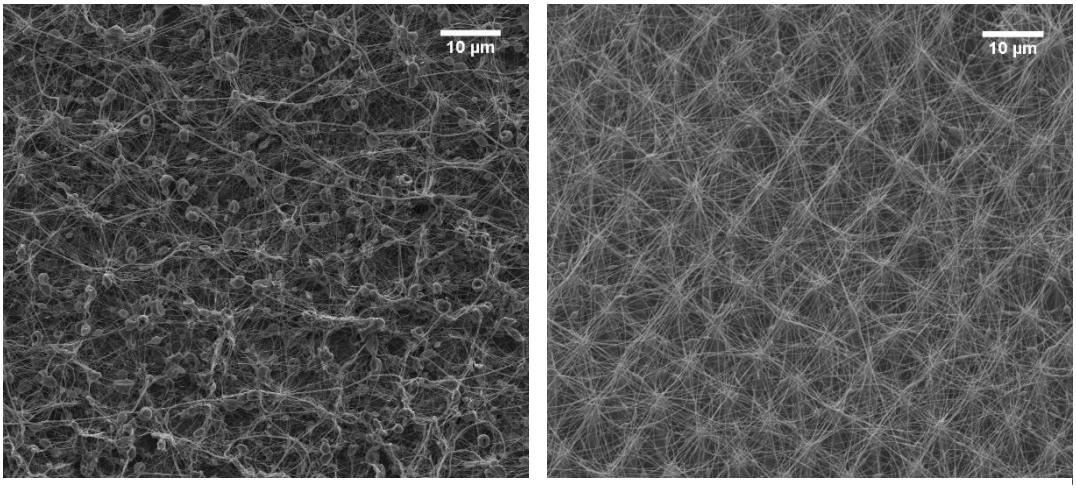

Figure 1.5: Comparison of electrospun polycaprolactone fibers. **(Left)** Deposition onto planar silicon substrate **(Right)** Deposition on silicon pillar grid array.

substrate. The right image shows deposition on a patterned silicon pillar grid array. The distinction in the morphology is evident, the deposition on the planar substrate shows random fiber orientation and large bead features interrupting the fibers. Deposition on the grid array shows some evident conformation to the grid architecture and more uniform, bead-free fiber features. This conformational fiber deposition is seen due to enhanced fields at the tips of pillars. There is a known report of deposition onto pillar features for a microfluidics application[47], but the dimensions of the pillar in that report are a larger scale (~400-500 μm) than shown in this work (~2μm).

1.6.6 Ambient conditions

Humidity and temperature are another set of electrospinning parameters that have been controlled for in several reports[48–50]. However, they were not controlled or investigated in this research. They have been studied primarily for the impact on the morphology of the fibers that are formed. Since the primary interest of the research was toward discrete features, the complication of a humidity and temperature-controlled enclosure was avoided, though it is possible they do impact the deposition of the materials and morphologies in this work.

1.7 Pulsed electrospray motivation and prior literature

The use of pulsed-field electrospray was hypothesized to have an impact on deposition results. The pulsed field is generated from a pulsed DC (direct current) time-varying high voltage signal. Segmented nanofiber deposition through use of a pulsed field have been demonstrated[51–53]. These reports used relatively low frequency pulses in the

single to ten hertz range. To our knowledge, pulsed-based electrospinning has not been reported in the range of frequencies greater than this. A goal in this research was to demonstrate tunable control over the deposition process via frequency and waveform parameters in the applied voltage used to generate the field for electrospinning.

To validate this approach to electrospinning, a lab-built high voltage amplifier was assembled using transformers to generate a periodic signal in the kilovolt magnitude range. This setup allowed for testing proof-of-concept that higher frequency (tens to hundreds of hertz) pulsed electrospinning is feasible, and the repeatability of using this setup. Depositions with frequencies as high as 500Hz were reliably achieved. A picture showing the internal electrical components is shown in the left panel of Fig 1.6. The right panel of the same figure shows an oscilloscope screenshot demonstrating the output signal given an input signal. The yellow color waveform is the input low voltage signal (here ~1Vpp) and the blue waveform is the high voltage output signal (~3.5kVpp). Clearly there is a lack of fidelity between the input and output signals, due to the transformer components used in the system.

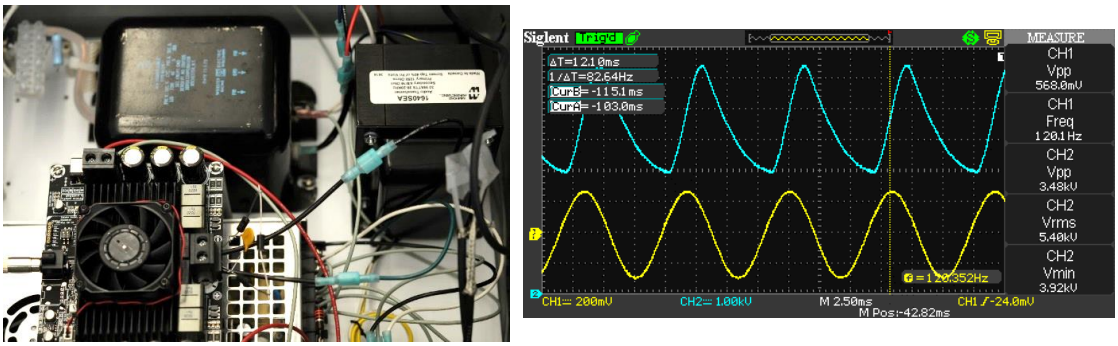

Figure 1.6: Early high voltage pulse system used **(Left)** Picture of main electrical components of system **(Right)** Oscilloscope waveform showing input waveform (yellow) and output waveform (blue).

Later in this project a Trek 10/10 high voltage amplifier was purchased by the project sponsor. This system provides 1,000:1 amplification of a low-voltage input signal with incomparably better fidelity than the lab-built transformer-based system and is operable at a much wider range of frequencies.

Chapter 2: Pulsed-field electrospray and characterization of discrete nanoparticles

2.1 Introduction

A motivation in this work was to develop methodology for electrospray deposition of discrete, oriented features. It was hypothesized that gas phase orientation of molecules could be selectively controlled through frequency and/or waveform parameters of a high voltage pulsed signal. This differs in approach to most electrospinning which uses a constant DC voltage to generate nanofibers. Initially, to conduct experiments in pulsed electrospray, we developed a transformer-based high voltage pulse system. This system was used successfully for pulsed depositions but had limitations and was eventually replaced with a commercial high voltage amplifier.

The material that saw the most use in this work for electrospray of discrete features was the protein fibrinogen. Fibrinogen is a large (~340 kDa) protein with a rod-like structure[54]. For this reason, it was selected early on as a material of interest to use in conducting experiments on pulsed deposition and orientability. Electrospinning of fibrinogen nanofibers has been reported by Wnek, et al. using a method to prepare a solution of fibrinogen in 1,1,1,3,3,3-hexafluoro-2-propanol (HFP)[12]. The process they reported used a stock preparation of the protein at a concentration of 83 mg/mL in minimal-essential-medium (MEM), prior to 9:1 dilution into HFP. Reports have been published on using electrospinning to produce biological-based nanofibers from fibrinogen[12] or collagen[11] and achieving results that mimic the extracellular matrix[55,56]. Research has also been conducted on the use of fibrinogen to fabricate biological-based bandages in applications for assisting wound healing[57].

Attempting to prepare fibrinogen for electrospinning, we found that using a solution preparation without MEM allowed for creation of non-fibrous, nanoscale-dimensional fibrinogen structures. These discrete feature morphologies lent themselves to being more applicable toward the study of electrical parameter effects on potential orientation during the deposition process.

2.2 Materials and methods

2.2.1 Materials

Fibrinogen (from bovine plasma) was purchased from Sigma (St. Louis, MO, USA). Bovine serum albumin from VWR (Radnor, PA, USA). Ammonium acetate from Mallinckrodt AR (Staines-Upon-Thames, Surrey, UK). Sodium chloride from EMD (Burlington, MA, USA). Polycaprolactone (Capa 6800) was obtained from Perstorp (Malmo, Sweden). Polyvinyl alcohol (99% hydrolyzed, MW 89kDA-98kDa) from Sigma-Aldrich (St. Louis, MO, USA). Purified DI water was obtained using a Milli-Q water purification system from Millipore (Burlington, MA, USA). Hexafluoro-2-propanol and trifluoroethanol were purchased from TCI America (Portland, OR, USA). Trifluoroethanol was also purchased from Sigma (St. Louis, MO, USA). Chloroform came from J.T. Baker (Phillipsburg, NJ, USA). Conductive adhesive copper tape was from 3M (St. Paul, MN, USA). Syringes used were from BD (Franklin Lakes, NJ, USA). Syringe needles were industrial dispensing tips from CML Supply (Lexington, KY, USA).

2.2.2 Development of lab-built transformer-based high voltage pulse system

2.2.2.1 System development and function

The lab-built setup was a cost-effective way to begin research into pulsed electrospinning (new high voltage function generators or amplifiers are an expensive piece of lab equipment). Mark Warner, formerly of the Oregon State Chemistry Department Electronics Shop, assisted in development, design and testing the transformer-based system in its first iterations.

The system functioned by using a low voltage input signal to generate a high voltage output in the kilovolt range (up to ~8kV). The primary component in the high voltage generation was a high voltage transformer. The high voltage signal, output from the transformer, was rectified using a high voltage diode to retain only the DC component of the signal. A 50MOhm resistor was added in series between the rectifying diode and the high voltage output of the system to act as a current limiter and keep output currents in the low 100μA ranges. The low-voltage signal was input to the system from a function generator (Tektronix CFG250). The signal was amplified using an audio frequency-range subwoofer amplifier and further stepped up by an audio frequency-range transformer (Hammond 1640SEA) to voltages in the 100VAC range. This is an appropriate magnitude of input voltage for the high voltage transformer, which was rated for operating with mains voltage on the primary coil.

Audio frequency range components were chosen for the circuit elements, where possible, to give the best fidelity frequency response over a range of frequencies. Though, that range was most notably limited by the high voltage transformer, which is generally not intended for use at frequencies other than standard 60Hz from mains. Although, it was

found that the transformer used for the system has a resonant frequency in the 500Hz range and a usable frequency range up to 1kHz. Usable frequency range being the range of frequencies where high-voltage output magnitudes sufficient for electrospinning were achievable. Usable frequency range does not mean that the waveform shapes generated across the range of frequencies were comparable between any given frequencies in that range. In fact, the greatest limitation of this system was the inability to control aspects of the pulse shape across a range of frequencies. The wave shape, peak-to-peak amplitude, and DC offset of the generated high voltage signal were all functions of the input frequency, waveform and amplitude. Therefore, it was usually not possible to maintain the same high voltage signal parameters at different frequencies and make exact comparisons. Because of this, the system did not allow for rigorous testing of electrospray behavior with directly comparable parameter sets at different frequencies, yet it did provide a means to investigate the feasibility of pulse-based electrospinning and demonstrate that it is readily practicable.

2.2.2.2 System iterations

Throughout its use the transformer system saw several design iterations and replacements of components. There were three different audio amplifiers used in different iterations of the system for the first-stage, low-voltage amplifying step. All were purchased as a developed amplifier board, not as individual amplifier integrated circuit components. Initially, a 68W LM3886 Class AB amplifier board by Yuan-Jing was used. This amplifier had thermal issues in use in the high voltage system and several were destroyed before it was decided to switch to a low-power/low-heat digital amplifier. A Sure Electronics AA-

AB31316 1x400W Class D Audio Amplifier was then used. Later, another Class D amplifier, the TDA 7492 amplifier board (purchased from Parts-Express), was used which was compatible with a smaller, lower-voltage power supply and the amplifier itself required less space. This would have allowed for developing the high voltage system into a more compact footprint, but this wasn't done before the transformer system's use was discontinued in favor of the Trek amplifier.

The first high voltage transformer used in this system was a Webster/Xerox Type 44324 transformer designed for use as an ignition in oil burning boilers. It was rated for a 7kV secondary voltage with a 115V primary voltage. It also had the secondary end-point grounded, with no center-tap, so only one connection to the secondary coil was accessible. This was later replaced with a "Steinville"/"Well" transformer designed for 5kV peak-to-peak voltage output. The schematic for this final iteration of the system is listed in Figure A.1 in Appendix A.2. Frequency range output responses were also characterized for maintaining specific output parameters and the details of this are listed in Appendix A.1. The Well transformer showed better peak-to-peak voltage magnitudes in the commonly used 100-500Hz frequency range than the Webster/Xerox transformer. However, the Well transformer was not potted in an insulator (like the Webster transformer) so there were issues reaching the same output voltages (greater than 5kV) as the Webster transformer. Static/arcing/breakdown noises were heard when trying to operate the system above 5kV. Testing the system in a low-light environment showed that arcing was occurring around uninsulated portions of the transformer. The Webster transformer was a more stable option

for higher voltage use. If the transformer-based high voltage system saw continued use, that would serve as a better component choice.

2.2.3 Solution preparation method development

One of the first materials electrospun on this project was the protein keratin in a mixture with polyethylene oxide (PEO) in trifluoroethanol (TFE), based on a preparation method reported in literature[38]. That solution was prepared with a 20 mg/mL concentration of keratin/PEO in TFE and rapidly coated (over several seconds) substrates during electrospray experiments (SEM image of results shown in Figure 1.2 in Chapter 1, section 1.5.1). Also, the morphology of this material was deposited as nanofibers. It did not respond to a pulsed DC waveform and segment into fibers. We sought to deposit material less rapidly and as discrete features so instead prepared fibrinogen electrospinning solutions at concentrations of protein at 5 mg/mL which is a significantly lower concentration than reported by Wnek et al. Initially, attempts were made to dissolve fibrinogen in TFE but it was not soluble in the solvent alone, so use of surfactants were studied to assist dissolving the protein. Solutions with 5mg/mL fibrinogen were prepared with 1 mg/mL surfactant in TFE. Surfactants used were cetyl trimethylammonium bromide (CTAB), capstone, and sodium dodecyl sulfate (SDS). The solutions were left to mix overnight on a rotisserie, but still appeared undissolved the next day. Solutions of 1 mg/mL protein were prepared with concentrations of 5, 25 and 50 mg/mL surfactant in TFE. But, none of the prepared solutions resulted in successfully dissolving the protein, though increased surfactant concentration appeared to decrease the size of the undissolved

particles. Fibrinogen could be dissolved at concentrations of 1, 5 and 10 mg/mL in either 9mg/mL NaCl (saline) or 100mM Tris-HCl pH 7.0. Attempts to electrospray 5 mg/mL fibrinogen from 100mM Tris-HCl were not successful and no spray behavior was seen. Ammonium acetate of 4.8 pH and 100mM was used to attempt to dissolve 1, 2.5, 5 and 10 mg/mL fibrinogen. Only the 1 mg/mL fibrinogen was successfully dissolved.

Fibrinogen solution preparation in TFE was attempted with additions of MEM. A ratio of 2 parts MEM to 8 parts TFE and 1mg/mL fibrinogen did not dissolve. Following Wnek et al and attempting to use HFP as the solvent system with 9:1 HFP to MEM with both 1 and 5 mg/mL fibrinogen was also not successful. Preparation of 1 mg/mL fibrinogen with 20 mg/mL SDS in HFP resulted in a clear, dissolved solution. Electrospraying this solution gave bead-like and granular morphology, likely influenced by the high surfactant to protein ratio.

Preparation of fibrinogen for electrospinning involved a several step solution preparation process. For the most successful preparation method, determined experimentally, the protein is first dissolved into a stock solution before preparation in HFP. The stock solution preparation method that proved the most successful was based from the manufacturer product page[58] and used saline (9mg/mL NaCl) and gentle agitation. Stock concentrations of the protein ranging from 10 mg/mL up to 200 mg/mL could be prepared in a saline solution. There was hesitancy to using saline-based solution preparation, due to incorporating addition non-volatile components to the solutions. As an alternative, ammonium acetate was substituted and stock solutions were prepared with this volatile salt instead. The stock preparation could then be diluted into the HFP solvent

system. Final dilutions of 5 mg/mL and 10 mg/mL were most frequently used. At higher concentrations there was significant crashing out from solution of dissolved material and resulting electrospray deposition morphology was large agglomerated particles. Preparation of fibrinogen stock solutions without salt additives was also possible, but higher concentration stock solutions was facilitated by using NaCl or ammonium acetate.

This solution preparation method was developed using fibrinogen but proved to be applicable for preparation of bovine serum albumin (BSA) solutions in HFP. In these cases, BSA was prepared in a phosphate buffered saline solution of pH 7.4 and diluted to final concentration of 5mg/mL in HFP. Deposition of this solution showed quite comparable morphologies to fibrinogen deposition. It is shown in Chapter 3, section 3.5.1.

2.2.4 Parameters used for electrospray deposition

Initially the solution preparation of 2 mg/mL fibrinogen (from 10 mg/mL stock in DI H_2O) was the primary approach used for electrospray. However, the preparation to either 5 mg/mL and 10 mg/mL (from 200 mg/mL stock in 9 mg/mL ammonium acetate) was used the most extensively, due to it being a more reliable solution to work with, having a more rapid rate of deposition during electrospray, and generating more discrete deposited morphologies.

Electrospinning of fibrinogen nanoplates was most successful at 1.5kV-2kV per cm needle-to-collector distances with the optimized deposition distance being 3cm with 5.5kV applied potential. Unless otherwise noted, fibrinogen samples were prepared by electrospray of the solution dispensed from a 3mL BD luer-lock tip syringe, fitted with a 22-gauge blunt-tipped syringe needle, onto a 1cm x 1cm square coupon of silicon wafer at a flow-rate of 50µL/hr. The silicon coupons were mounted and electrically grounded to a metal post using double-sided copper tape with a conductive adhesive. A good example of the deposition pattern on these substrates is shown in Figure 2.1 with a circular pattern. Deposition density was typically gradient from the center to the outer edge of the spray area. It did not always center on the substrate and in some cases would overlap the edge of the silicon.

Figure 2.1: Electrospray deposition onto 1cmx1cm silicon wafer coupons. Here mounted on pin stub holders prior to SEM imaging.

2.2.5 Silicon substrate cleaning procedures

Non-patterned silicon substrates (shown after use for electrospray in Figure 2.1) were cleaned prior to use. The method used sonication in solvents: acetone, methanol,

and DI H_2O. This step was done after silicon wafers had been diced into 1cm x 1cm coupons. Both variations on the cleaning procedure listed below were useful to remove some of the debris from the substrates that was left after wafer dicing.

10-minute per-step single sonication with rinse:

1. 10-minute sonication in acetone
    a. Rinse substrates individually with acetone
2. 10-minute sonication in methanol
    a. Rinse substrates individually with methanol
3. 10-minute sonication in DI H_2O
    a. Rinse substrates individually in DI H_2O
4. Dry substrates individually using dry nitrogen gas

5-minute repeat sonication:

1. 5-minute sonication in acetone
    a. Replace acetone and repeat sonication
2. 5-minute sonication methanol
    a. Replace methanol and repeat
3. 5-minte sonication in DI H_2O
    a. Replace DI H_2O and repeat
4. Dry substrates using dry nitrogen gas

2.2.6 Image based feature characterization

2.2.6.1 Image collection

Scanning electron microscopy was used for collecting images of electrospun samples. The scanning electron microscope used was a FEI Quanta 600 in the Oregon State University Electron Microscopy Lab. Samples usually were prepared with sputter-coating prior to imaging to address charging and poor contrast issues as most of the deposited materials worked with were non-conductive. Sputter-coating with Au/Pd was generally done for 35 seconds. Most images were collected with a 5kV accelerating voltage. The

relatively low voltage was used due to the electrospray deposited materials generally having sensitivity to higher accelerating voltages.

2.2.6.2 Image segmentation and feature characterization

Image segmentation is a nebulous process which is facilitated by obtaining proper images as much as the proper application of processing techniques. Images need to be taken with consideration toward the later application of segmentation. Many images obtained throughout the collection of data for this work do not have high contrast. Without this, the images' histograms do not have distinct peaks. The images cannot be segmented by a simple pixel intensity threshold approach alone. More complex segmentation algorithms must be applied, which still require tuning to generate the desired results; this is the nature of image segmentation. Only qualitative observations can be made without successful application of segmentation to extract quantitative measurements from images. Still, there is variability in the results obtained from different approaches to segment and extract quantitative measurements from the images.

The Feret diameter was considered the most relevant measurement of the electrosprayed features, since it is measured as the longest distance across a particle feature and provides a means to measure the distribution of electrosprayed particle sizes. Several segmentation algorithm approaches were applied to determine their variability to the resulting size measurements. ImageJ and FIJI software were used for image processing to measure the Feret diameter of deposited nanoparticles using the Particle Analysis tool in the BoneJ plugin extension to FIJI. The processing steps of filtering, segmentation, binary

operations (erode, dilate, hole fill, watershed) and particle size analysis were all performed within ImageJ. The generated arrays of Feret diameter measurements were exported to MATLAB for computing a distribution plot of size-binned feature measurements (particle size histogram). MATLAB was also used for plotting graphs of the data. A more comprehensive script could be implemented, entirely using MATLAB for image processing, segmentation, extraction of measurement data and graphing of this data. But, that was not achieved for this work.

The image in Fig. 2.2 is electrospray deposited polyvinyl alcohol (PVA) used in developing image segmentation approaches for making quantitative measurements from SEM image data collected during this research. The image shows some distinct contrast

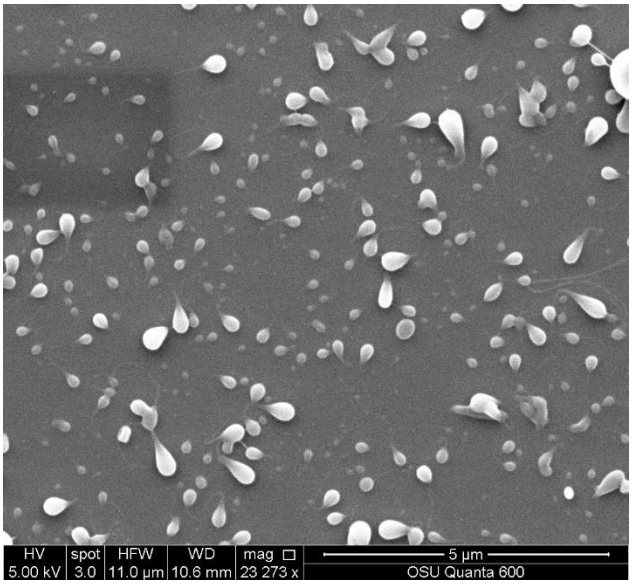

Figure 2.2: Electrospun polyvinyl alcohol (PVA) particles.

between the background and the deposited features. However, there are not separate peaks in the histogram, so a simple intensity threshold is not applicable. A median filter of 2.0-pixel size was used to address background noise in the image. Three segmentation

algorithms were applied to compare results: unsupervised K-means, supervised Hidden Markov Model, and supervised K-means. These segmentation approaches operate on pixel intensity and separate the image into regions by labelling as one of a pre-defined number of classes. Three color classes were used with each segmentation approach. Each resulting array of feature size measurements were sorted into size distribution bins of 50 nm width (~5 pixels for SEM images recorded at 11μm horizontal field width (HFW) and ~10 pixels for an HFW of 5 μm). Features with a Feret diameter ~20nm were removed, due to these likely being noise features from segmentation and features of this size were not visually recorded in hand measurements, so they are not expected to represent deposited features. The size histogram counts were normalized to the total number of counts to allow direct comparison between size histograms from different samples with differing numbers of total feature counts. Between the filtered, size-binned Feret measurements from different segmentation approaches the mean and error of the percent of binned counts was computed. The results of the three segmentation methods applied to the image in Fig. 2.2 is shown by the graph in Fig. 2.3. There is variation in the size measurement distribution based on the segmentation approach used, introducing possible error. Ultimately, the choice was made to use the automatic k-means segmentation approach. The supervised k-means cluster and hidden markov model both required training the algorithm on each image to be segmented. To process multiple images from multiple samples, this was not feasible from a user perspective. Both user time and, by involving a user, the possibility to introduce inconsistencies in class selection. The automatic approach allowed the incorporation of the

tool into an ImageJ macro process to crop, filter, segment, apply binary operations, and measure particle features.

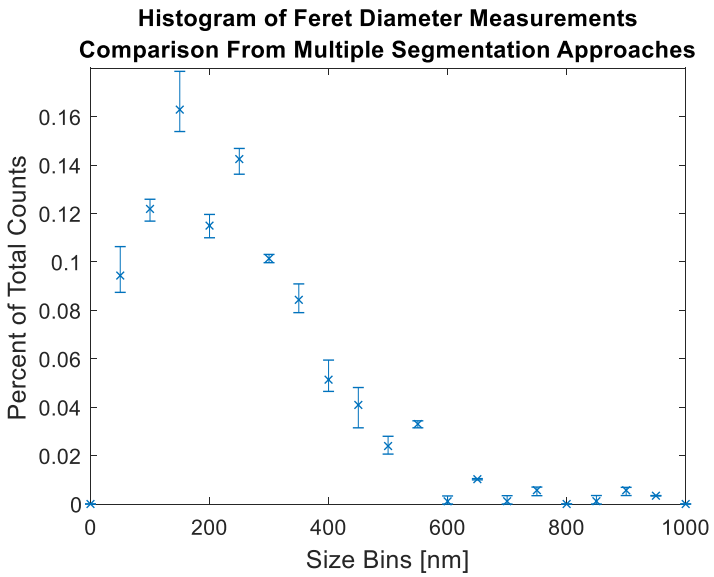

Figure 2.3: Mean size distribution of electrospun polyvinyl alcohol (PVA) particles with error shown between comparison of different segmentation approaches.

2.3 Results and discussion

2.3.1 Electrospray deposition of discrete nanomaterials

Throughout this research has resulted in the ability to deposit discrete feature morphologies from various materials of protein or polymer. Examples of these are shown in Fig. 2.4. These features have all been deposited using low concentrations of material in solution (5 – 10 mg/mL) which is conductive to depositing these morphologies. In cases where the morphology and size of the deposited features was studied, the collection substrate used was a 1cm x 1cm coupon of silicon wafer mounted on an aluminum foil backing (3cm x 3cm). The silicon coupon was attached to the foil with a double-sided

conductive adhesive copper tape and the foil was mounted on a grounded metal post using the same tape.

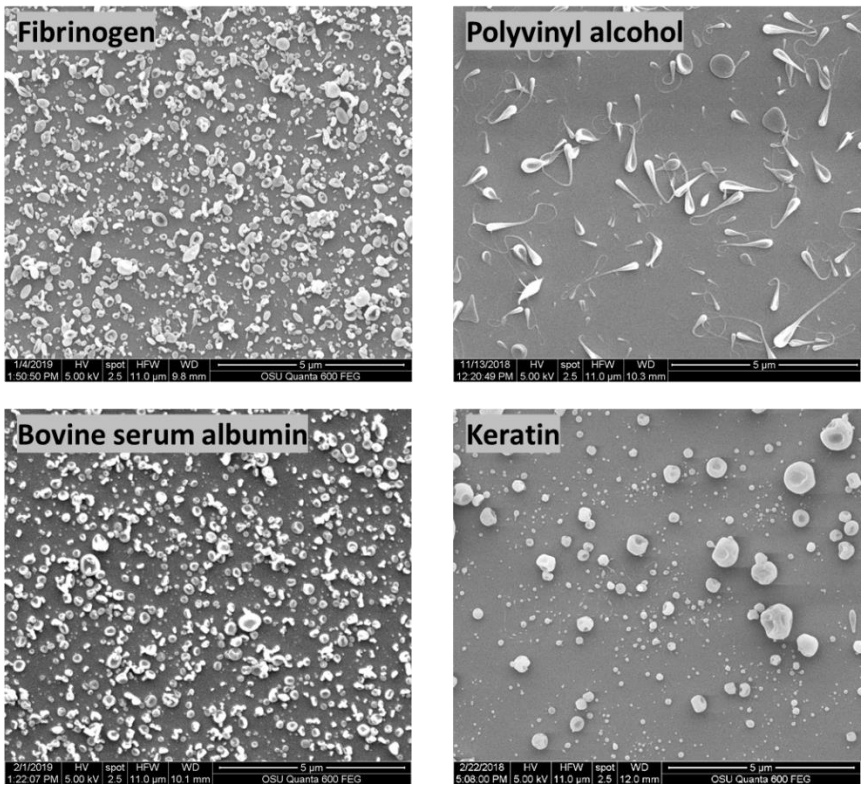

Figure 2.4: Electrospun proteins (fibrinogen, bovine serum albumin) and polymer (polyvinyl alcohol).

Electrospray was demonstrated with DC deposition when a sufficient field strength was reached. Operating field strength was dependent on the solvent system used. Volatile organic solvent systems required strengths in the range of only 1.5-2 kV/cm (hexafluoro-2-propanol, trifluoroethanol). Whereas when working with aqueous systems 2 kV/cm was typically the lowest possible field strength where electrospray occurred. The DC voltage where the onset of stable electrospray of fibrinogen began was recorded at several working distances listed in Table 2.1.

Table 2.1: DC electrospray onset voltage for deposition of 10mg/mL fibrinogen in HFP.

Electrospray of fibrinogen	**2cm**	**3cm**	**4cm**
Onset Voltage	4 kV	4.5-5 kV	6 kV
Field Strength	2 kV/cm	1.5-1.67 kV/cm	1.5 kV/cm

The required field strength was observed to decrease with increased deposition distance in electrospray of this solution. A wider range of distances was possible for electrospray. Deposition at a distance shorter than 2cm was usually not practical because unevaporated solvent could be collected. Deposition could also be achieved at distances greater than 4cm (by adjusting voltage appropriately) but at longer distances the spray area was typically larger than the substrate. This 2cm-to-4cm needle-to-collector distance range was the space predominantly used.

Parameters could be noted for electrospray deposition with a pulsed DC, time-varying signal in several ways. The transformer system initially used had a frequency dependent peak-to-peak voltage. While this behavior was characterized, the RMS voltage of the signal was used to make comparisons between electrospray at different frequencies. Depositions were achieved at frequencies ranging from 60Hz to 500Hz. Though, in the upper range of frequencies, the peak-to-peak voltage was diminished, compared to lower frequencies. Fibrinogen was first stably deposited using a 5.3kVrms, 120Hz signal at a 3cm deposition distance. This agrees with (several hundred volts above) the minimum onset DC voltage for this distance, which was determined later (listed in Table 2.1).

After transitioning to use the Trek 10/10 high voltage system, noting and controlling more parameters of the signal was appropriate because these aspects of the signal parameters were fully adjustable with the Trek amplifier. Peak-to-peak voltage and DC component offset are a reproducible description which can be set at different frequencies.

2.3.2 Electrosprayed morphologies and relation to solution parameters

The earliest successful technique used in this research to deposit protein nanoparticles was by preparing fibrinogen at a concentration of 10 mg/mL in DI H_20 and allowing to dissolve at room temperature over a period of several days. The stock solution was then diluted 1:4 in HFP for a final concentration of 2 mg/mL of fibrinogen. This solution could be readily electrosprayed and is shown in Fig. 2.5 after deposition on a coupon of silicon wafer. Electrospray deposition of this fibrinogen solution showed a distinctly flake-like morphology and was centered in localized regions which showed a

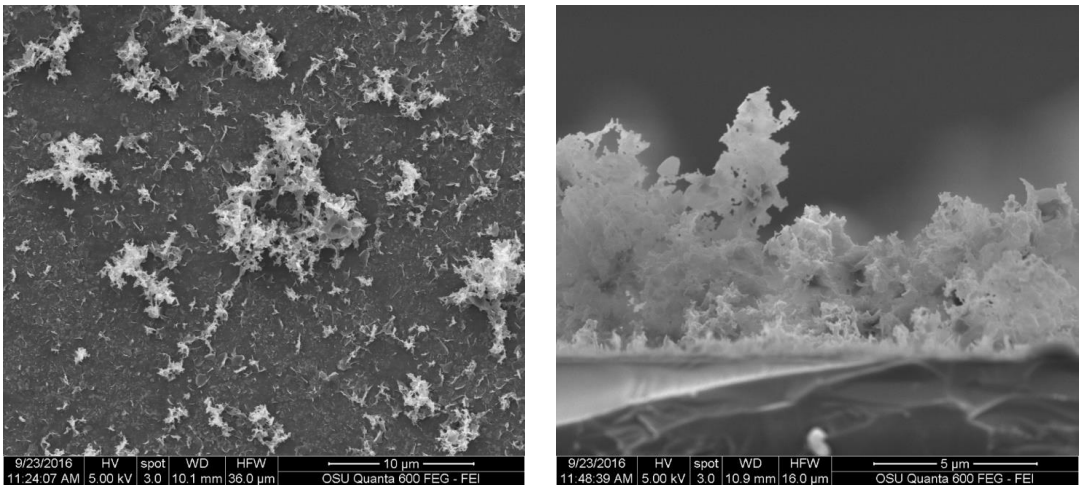

Figure 2.5: Electrospun 2 mg/mL fibrinogen on Si coupons. **(Left)** Top down view. Scale at 10um **(Right)** Cross-sectional view of cleaved wafer sample. Scale at 5um.

structure oriented upward from the substrate surface. The depositions shown in the figure were performed using the transformer based high voltage system (detailed in section 2.2.2) at a 120Hz pulsing waveform with an effective 5.3kV DC component at a needle-to-collector distance of 3cm with a dispensing flow rate of 50 µl/hr.

Electrospraying fibrinogen solutions with 2 mg/mL dilutions in HFP, from varied stock solution concentrations, showed varied morphology results. The results are shown in Fig. 2.6 of the resulting morphologies from electrospray of solutions with 50 mg/mL, 90

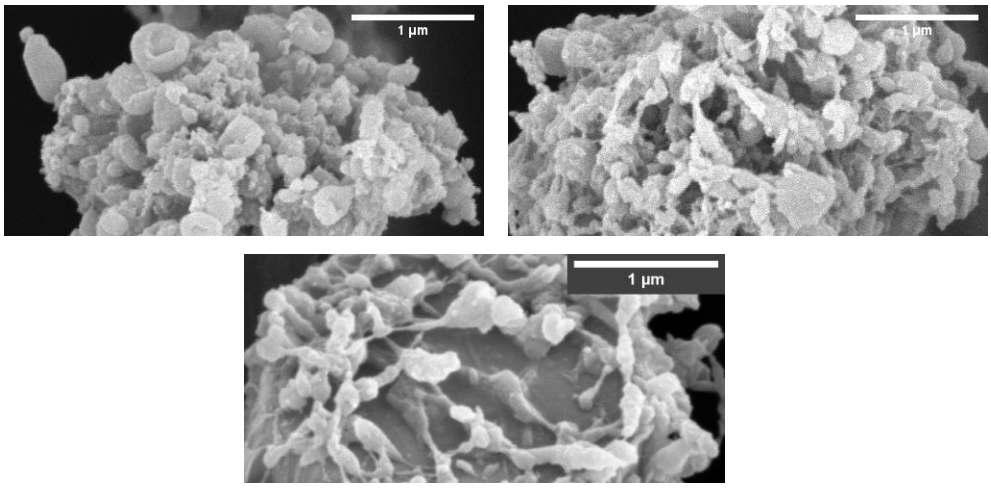

Figure 2.6: Electrospun 2 mg/mL fibrinogen on Si substrates. Dilutions prepared from stock concentration into HFP solvent system. **(Left)** From 50 mg/mL stock **(Middle)** From 90 mg/mL stock. **(Right)** From 200 mg/mL stock. Scale bars are at 1um.

mg/mL and 200 mg/mL wt. stock solutions diluted to 2 mg/mL final concentration of fibrinogen in HFP. The benefit of the higher concentration stock is a reduced ratio of NaCl to protein in solution, since all concentrations of protein were prepared using the same concentration of NaCl (saline, 9mg/mL). However, none of these results showed distinctly discrete morphologies. Preparation of the dilute solution at 10 mg/mL in HFP from 200 mg/mL stock in saline gave a distinctly different resulting morphology shown in Fig. 2.7,

also deposited using the transformer pulse system. These results show a “cupped” shape. There is a definite distribution in particle size, but features tend to the sub-micron range and most heavily in the 100-300nm range.

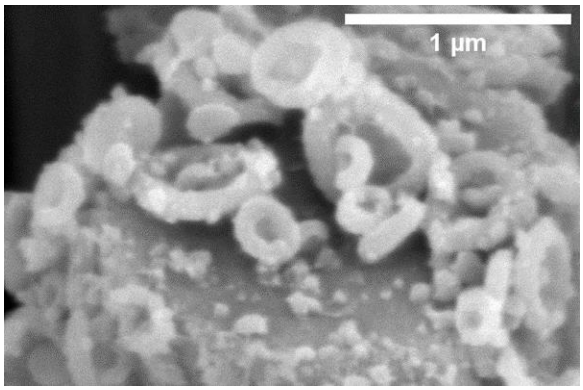

Figure 2.7: Electrospun 10 mg/mL fibrinogen from 200 mg/mL stock. Scale bar at 1um.

2.3.3 Voltage parameters effect on electrospray of fibrinogen

Electrospray of fibrinogen nanoparticles showed variation in deposition comparing pulsed DC to DC deposition. The parameters compared were DC at a 6kV magnitude voltage and pulsed 50% duty cycle square wave with 3kV peak-to-peak voltage (minimum at 3kV, maximum 6kV). These pulsed depositions were done using the Trek high voltage amplifier. By choosing a minimum voltage at half of the maximum, there should be no electrospray occurring during that portion of the period of the pulsed waveform. Difference in deposition density is apparent between DC and pulsed DC in the SEM images shown in Fig 2.8. All samples were prepared using a 30 second deposition, so this density difference between DC and pulsed parameters can be accounted for by the periodicity of the pulsed DC waveform, which has less time over the deposition where there is sufficient field to cause electrospray.

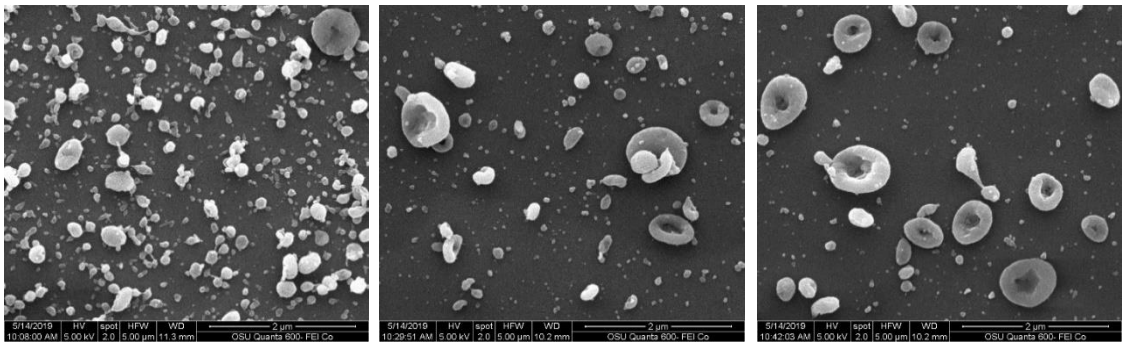

Figure 2.8: Electrospun 5mg/mL fibrinogen on Si coupons. Scale bars 2um **(Left)** ES at DC **(Middle)** ES at 100Hz **(Right)** ES at 500Hz

Image processing and segmentation in ImageJ was used to make quantitative feature size measurements and comparisons between the images. The process used was: median filter (2.0-pixel size), background subtraction, segmentation (automatic 3-color-class k-means cluster), threshold to binary, binary operations (erode, dilate X2, hole fill, erode, watershed), and finally BoneJ particle analysis to collect Feret diameter measurements. To compare the pulsed DC and DC parameters results, five samples of each parameter set (DC, 100Hz pulse, 500Hz pulse) were prepared. The images in Figure 2.8 are an example from each parameter set. From each sample three images were collected and processed with the image segmentation. The array of measurements from each of the three images of a sample were combined and counted into sized bins of 50nm width (the first bin is 0-50nm, though 20nm and below sizes are not considered). The counts in each bin was normalized by the total number of measurements made across the three images. There is quite significant variability in the distribution of small features (50-100nm) between the DC deposition samples. The depositions with pulsed DC are consistent across the size bins. In the 100-250nm size range the DC depositions show greater fraction of distribution than the pulsed DC parameters.

Based solely on visual inspection of the images, there are evidently more of the largest feature sizes present on the pulsed DC deposited samples. This doesn't show in the distribution plotted in Figure 2.9, due to the graph scale being skewed toward high fraction of distributions at the lower feature sizes. Viewing the numerical data which is plotted in the graph reveals that the upper size features (500-100nm) are seen more in the pulsed DC depositions than the DC, though these feature sizes are still a small minority compared with the amount of small feature sizes. This numerical data is included in Table B.1 in Appendix B, section B.2.

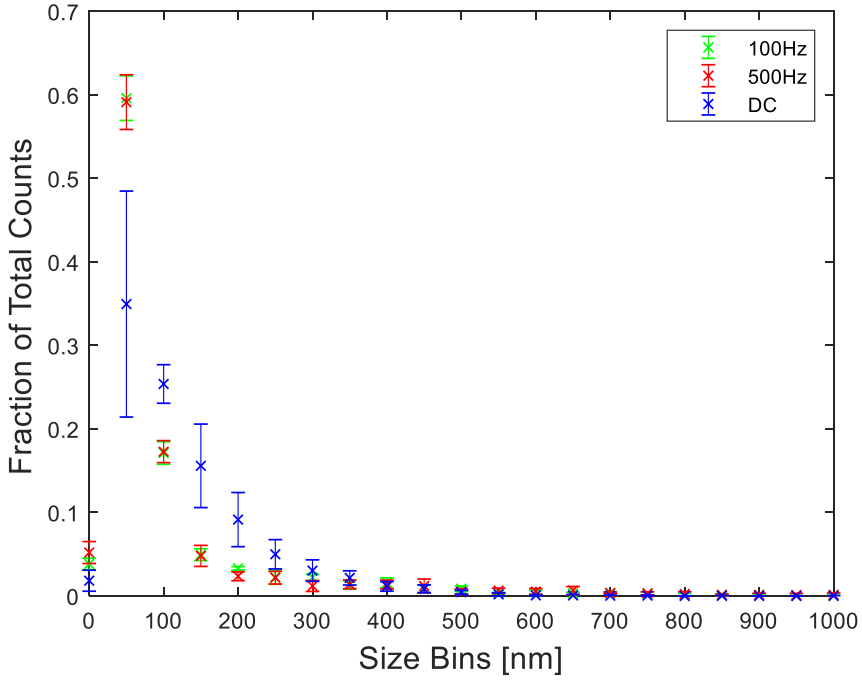

Figure 2.9: Size distribution of electrospun fibrinogen at DC, 100Hz and 500Hz parameters. Size bins are 50nm in width.

Chapter 3: Electrospray deposition of protein nanoparticles for enhancing performance of a microfluidic blood plasma separation device

3.1 Introduction

We have demonstrated the ability to electrospray protein as discrete nanoparticles. There are multiple proteins and enzymes involved in the blood coagulation cascade which could be considered for electrospray to increase blood coagulation on a separation device[59]. The ability to electrospray fibrinogen, a protein involved in blood coagulation, motivated the application of electrospray deposition for enhancement of the performance of a microfluidic blood plasma separation membrane device. Electrospinning has been reported in literature[60–63] for blood separation applications by fabrication of electrospun filtration membranes but, to our knowledge, no publications exist on electrospray deposition of blood coagulation chemistries for blood plasma separation applications.

3.2 Motivation for application to a blood plasma separation device

Fibrinogen is a protein which is involved in the blood coagulation cascade. During blood clotting fibrinogen is cleaved into fibrin by the enzyme thrombin and polymerizes as fibrin[54,64]. Fibrin forms as fibers, which act to bind up red blood cells in the blood and form clots[54]. We were motivated to electrospray fibrinogen nanoparticles toward an application with a microfluidic blood plasma separation device developed from glass microfiber membrane in Remcho Research Group as part of a student's thesis work[65]. The goal was to enhance coagulation by introducing additional coagulation chemistries. The microfluidic membrane device does not rely on instrumentation and is applicable to quantitative point-of-care analysis; which facilitates its employability in resource limited

areas without access to clinical laboratories or as an easy-to-use, single-use analytical device for in-lab applications[65]. It relies on hydrophilic surface chemistry to cause wicking fluid flow on the membrane and is single-use for this reason – after use with fluid, it will no longer wick fluid. Electrospray is a compelling technique for modifying the device after fabrication, since the membrane is not exposed to any solvent during the deposition process which avoids altering its hydrophilic surface chemistries.

3.3 Function of blood plasma separation membrane device

The membrane device is capable of separating blood samples into two fluid components: the red blood cell and plasma (or serum) components[65]. Whether serum or plasma is the separated component in the device depends on whether the blood has been treated with an anticoagulant. Serum is fluid remaining after blood clotting and is a component of plasma but contains no coagulation chemistries (they have been involved in the blood clotting)[66]. Plasma separates from blood which has been treated with an anticoagulant, so the coagulation chemistries remain in the liquid[66]. Fresh blood samples will coagulate on the device, so the fluid which separates from the red blood cell containing fluid will be serum. Anticoagulant treated blood samples will be separated as red blood cell fluid and plasma fluid components.

Separation of these fluid components is achieved through lateral flow of the fluid sample on the membrane device. Initially, glass microfiber is hydrophilic, but in the device fabrication, the membrane is filled with the polymer polycaprolactone (PCL) and rendered hydrophobic[65]. Fluid flow channel features are patterned into the device via selective

oxygen radical exposure (ORE) through a mask which defines the desired features. This ORE step renders the exposed areas hydrophilic via surface energy activation. The result is a hydrophilic channel feature patterned into a hydrophobic membrane device. Fluid introduced into a circular sample zone at one end of the channel is wicked by the hydrophilic surface to flow down the channel. When a blood sample is introduced to the membrane the subsequent flow along the channel results in a retention of the red blood cell fluid component within the matrix more than the plasma (or serum) component. This allows for assay to be performed on the less retained plasma (or serum) component[65].

Blood tests were performed on two styles of separation membrane. The first device (shown in Fig. 3.1) has a patterned loop structure, with surface flow on both top and bottom of the membrane. After a blood sample is introduced on the top surface, it first flows through a via to the bottom surface, then flows along a channel on the bottom surface before finally returning to the top surface through another via and flowing along a channel to an assay region. Electrospray deposition was done onto the bottom surface flow channel. The second style of device (Fig. 3.2) does not use any via structure and has separative flow in a surface channel on one side of the device.

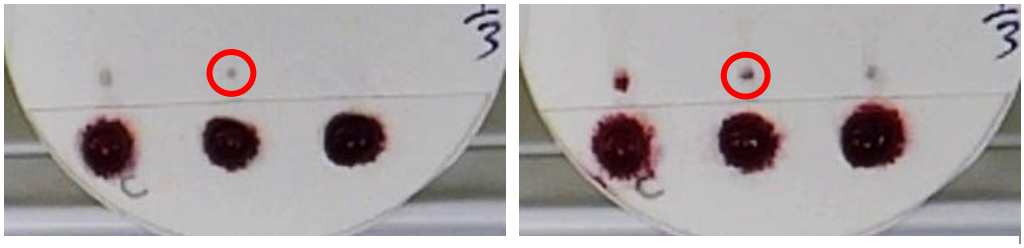

Figure 3.1: Loop structure blood separation device **(Left)** Serum (clear fluid circle) can be seen reaching the top of the via, returning to the top surface **(Right)** At a later point in time, red colored fluid (containing red blood cells) is now reaching the top of the via.

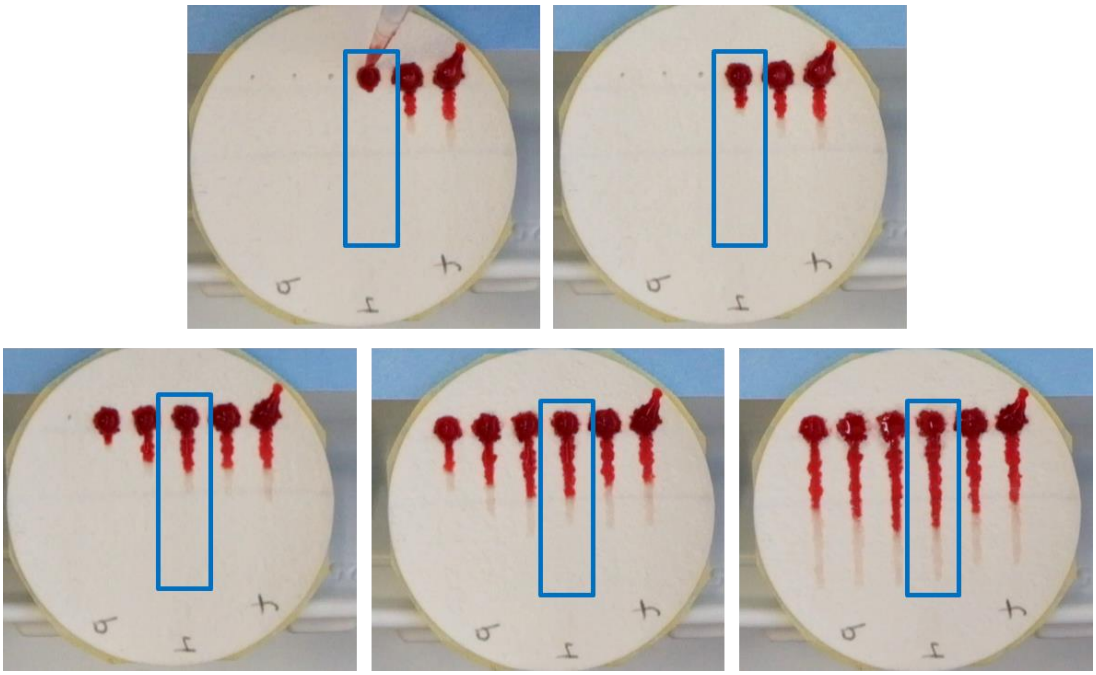

Figure 3.2: Separative blood flow on a single-sided membrane device depicted at several points during the process. **1)** Sample is introduced **2)** Some separation of the fluid components is visible **3)** The separated plasma component of the sample has reached the end of the functionalized region **4)** Red blood cell fluid component has reached the same point **5)** After flow is complete

3.4 Methods

3.4.1 Electrospray onto membranes

Conducting these experiments required devising a setup for electrospraying onto the membrane devices. Typical electrospray collectors are conductive (metal foil) or semi-conductive (silicon) materials. By mounting the membrane onto a grounded conductive backing we were able to generate electrospray that collected on the membrane. Masking off specific regions of the channel on the membrane device allowed for functionalizing selected regions with the fibrinogen nanoparticles. Shown in Fig. 3.3 is comparison of the membrane device with and without nanoparticle functionalization, demonstrating how these features appear (on the micro-scale) when deposited onto the device using the

electrospray technique. No macro-scale images of devices after functionalization with electrospray are included, because the glass microfiber membranes are white and electrosprayed fibrinogen also has a white appearance.

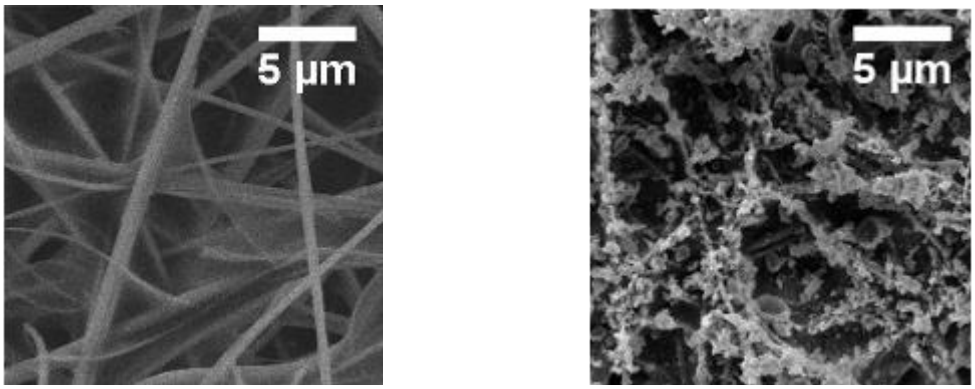

Figure 3.3: (Left) Un-modified, control membrane **(Right)** Membrane modified with electrospray deposited nanoparticles

3.4.2 Measurement of device performance

Flow performance across the masked surface deposition region was compared between functionalized and non-functionalized channels (control). The rate of fluid flow was measured as the difference in time between the two separated fluid fronts reaching the same point on the channel, at the end of the functionalized region. The clear plasma (or serum) component flows faster, so the time between this component reaching the end of the surface deposition region and the red blood cell component reaching the same point is measured as the separation time and indicates the efficiency or strength of the separation. Comparing the separation time between channels functionalized with the nanoplates versus un-functionalized (control) channels shows how the electrospray functionalization affects the flow behavior. A drawing of the later surface flow separation is shown in Figure 3.4, indicating the separative flow over the functionalized region. To minimize variation in

results due to the variability in the device fabrication, control channel flow was measured on each device. The separation time on control channels was used to normalize the flow time on functionalized channels on each device. Then, normalized separation time was comparable between devices.

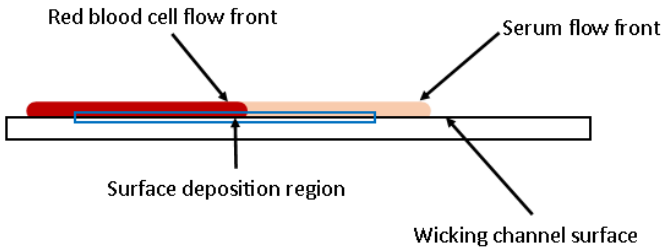

Figure 3.4: (Left) Diagram of blood separation behavior on lateral surface flow channel.

3.5 Results and discussion

3.5.1 Protein materials deposited

Another comparison method used in these experiments was the deposition of a protein not used in blood coagulation, bovine serum albumin (BSA), to determine how fluid flow is effected by a material with similar morphology to the fibrinogen nanoplates. Shown in Fig. 3.5 is comparison of electron microscope images of deposition of BSA and fibrinogen nanoparticles on the membranes.

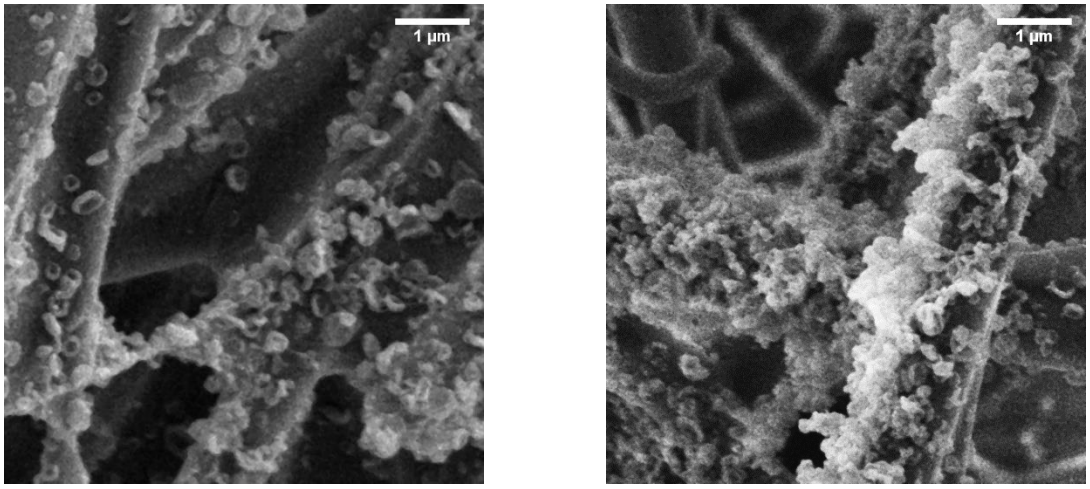

Figure 3.5: (Left) Fibrinogen nanoparticles deposited on the membrane device. **(Right)** Deposited bovine serum albumin nanoparticles.

3.5.2 Test with control fluid

If fibrinogen specifically interacts with a fresh blood sample, and causes an increase in coagulation, then increased separation time (between the plasma and red blood cell component) would be seen with only the fibrinogen functionalized channels and not those functionalized with BSA. To see how fluid flow is generally impacted, phosphate buffered saline (PBS) of pH 7.4 with a color dye was used to compare the affect on the flow times of a non-blood fluid sample across control, fibrinogen functionalized, and BSA functionalized channel regions. These flow time data are shown in Fig. 3.6 with flow times on fibrinogen and BSA coated channels normalized to the control flow time. Though there is variation in the mean flow time, there is not a significant impact due to the presence of electrospray deposited protein nanoplates.

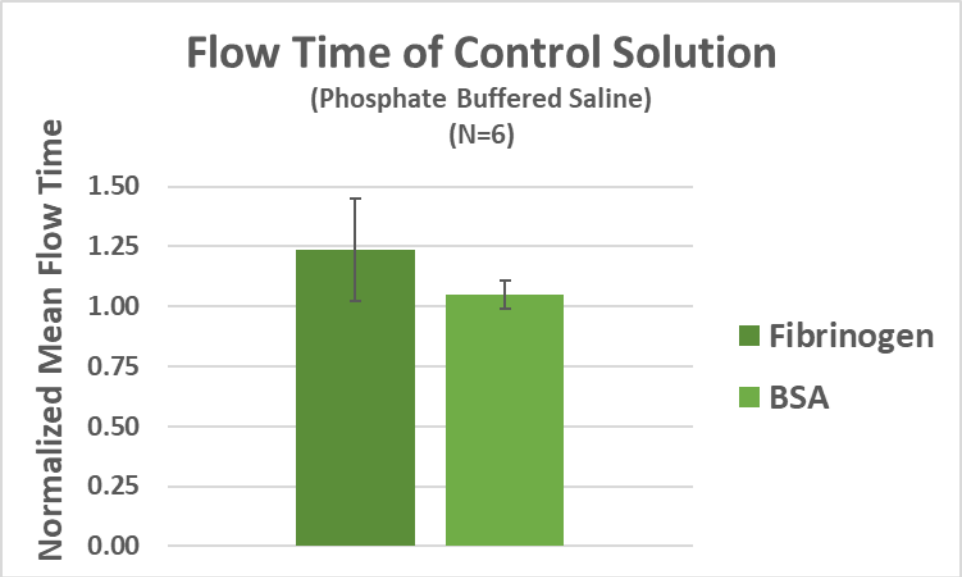

Figure 3.6: Mean flow time of a non-blood fluid sample across protein nanoplate functionalized and control regions of the separation membrane.

3.5.3 Device testing with blood samples

Blood samples used for the blood separation performance testing were collected from canine sources. Fibrinogen deposited on the membrane devices was sourced from bovine plasma. It should be noted that this cross-species aspect is not an issue, generally any mammalian fibrinogen can interact with any mammalian thrombin in coagulation[58]. The impact of protein nanoplates on separation performance was compared with both EDTA-treated and fresh blood samples. EDTA is a chelating agent for metal ions, such as calcium, and is used as an anti-coagulant treatment for blood samples[67]. It functions by binding to calcium[67] in the blood, which is a catalyst for the conversion of fibrinogen to fibrin. This cuts off the route for fibrinogen's involvement in blood coagulation. If fibrinogen nanoplates deposited onto the separation device through electrospray can interact with the blood sample and affect coagulation, there should be a more significant impact on the flow of a fresh blood sample than on an EDTA treated sample.

3.5.4 Blood separation results

What as observed, however, was a remarkably similar impact on the flow time of both fresh blood and EDTA treated blood, when blood separation was done on a fibrinogen functionalized membrane channel. These flow time results are shown in Figure 3.7, with the flow times in the functionalized channels normalized by the flow time of the control (non-functionalized) on the same device.

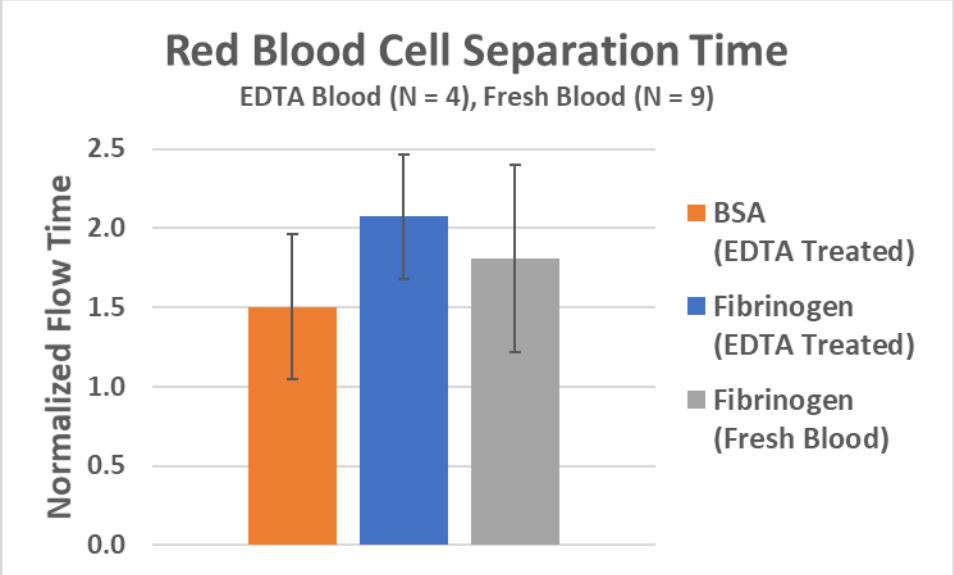

Figure 3.7: Separation time between RBC and plasma fluid components testing with EDTA and fresh blood samples on BSA and fibrinogen functionalized channels, normalized by control.

This similarity in flow behavior is indicative that the fibrinogen may not specifically affect coagulation of the blood. Membrane channels functionalized with BSA nanoparticles also show an increase in the flow time, though not as significantly as compared to the fibrinogen functionalized. Shown in Fig. 3.8 is the compared flow times

of only the plasma component of an EDTA treated blood sample on fibrinogen versus BSA functionalized channels.

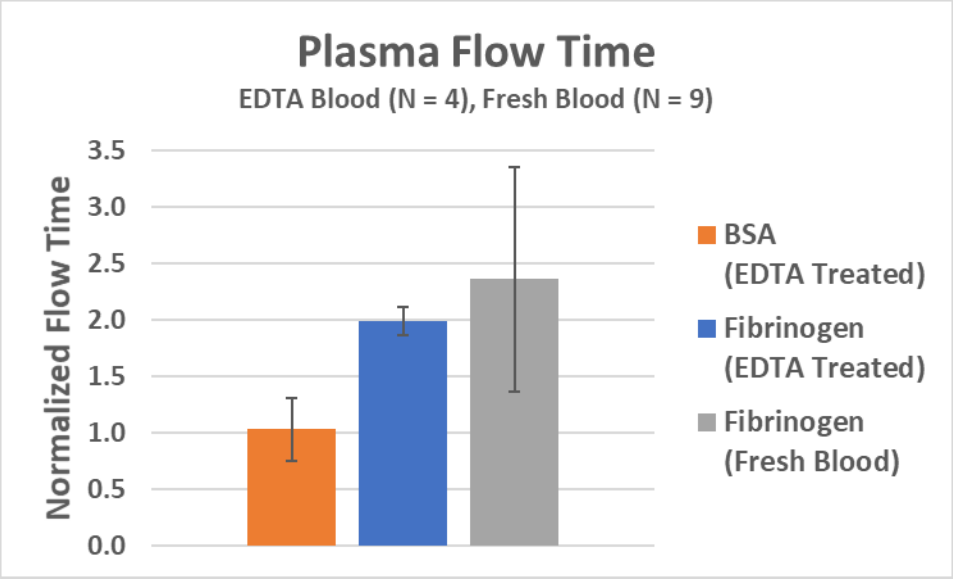

Figure 3.8: Flow time of plasma fluid component on BSA and fibrinogen functionalized channels, normalized by control.

This was measured as the time from introduction of the sample to the device to the time when the plasma fluid flow reached a marked point on the channel. Again, these flow times are normalized to the flow time of sample on the control (non-functionalized) channel. In this case, the flow time on the fibrinogen coated channel is about twice that of the control. The flow time of the plasma component on the BSA functionalized region does not differ significantly from the control flow time.

Since fibrinogen deposition shows a similar effect on the separative flow of both fresh and anticoagulant-treated blood samples, it is not conclusive that the protein is impacting coagulation. While a similar effect from the fibrinogen is also seen on the flow time of the plasma, the BSA does not notably impact the flow. So, it is also not conclusive

whether the protein nanoparticle features are simply impeding the flow of the blood sample.

Chapter 4: Electrospray deposition of the glucose oxidase enzyme for an electrochemical glucose sensor application

4.1 Introduction

A primary goal in this research in electrospinning/electrospray was to develop the ability to manipulate and control the deposition of discrete nanomaterials. Specifically, the goal was to achieve tunable control over the orientation of deposited features via frequency and waveform parameters of the high voltage applied during the electrospray process. Proteins such as antibodies and enzymes are of interest for application of this study, because orientation is a critical factor in the efficiency of antibody-antigen or enzyme-substrate binding. Both have an active site which must be oriented favorably to allow interaction with an analyte[68], [69]. Comparing signal response between sensors prepared using different functionalization approaches is a compelling method to study the effect of electrospray parameters.

4.1.1 Electrospray for sensor functionalization

Electrospinning has been applied for the purposes of electrode functionalization or fabrication. Non-enzymatic electrospun fiber sensors have been demonstrated for glucose detection[23,70–72]. Other electrospun fiber sensors for gas contaminants such as carbon monoxide and hydrogen sulfide[25,26,73] have been fabricated using electrospinning. Moisture sensitive electrospun materials have been applied to humidity detection[8,22,74]. Few have reported on direct electrospinning or electrospray of glucose oxidase enzyme incorporation into electropun material for development of glucose sensors[75–77].

The controlled deposition of the enzyme glucose oxidase (GOx) was studied for the application of electrochemical glucose detection. Prior literature has reported on techniques involving electrospinning/electrospray and GOx functionalization. However, most of these reports use electrospinning to fabricate a nanofibrous membrane mat and subsequently immobilize the enzyme to the fiber in liquid phase[78–81]. Ge et al. demonstrated retention of enzyme activity after electrospray deposition but notably, Ren et al. demonstrated deposition of GOx incorporated into solution with the polymer polyvinyl alcohol (PVA) for an electrochemical glucose sensor application[76]. However, the deposited morphology is continuous fibers interrupted by bead morphologies. This is less desirable for a goal of affecting orientation, since features are not discrete in the fibrous morphology and attachment by continuous fibers could interfere with orientability.

4.1.2 Replication of reported method: enzyme functionalized fibers

Incorporation of 1mg/mL GOx into 10 mg/mL PVA (99% hydrolyzed) in an aqueous solution was attempted for surface functionalization of an electrochemical sensor. The resulting morphologies shown in Fig. 4.1 are comparable to results shown in Fig. 2(c) in Ren et al. The resulting morphology achieved in this work has notably smaller bead and fiber dimensions. We did not follow the full procedure they used with glutaraldehyde (GA) vapor exposure to crosslink the PVA and GOx. As a result, the sensor demonstrated a decaying signal during the additions of glucose to the electrochemical sensor environment. This is likely due to the solubility of the PVA fiber support matrix without the use of GA vapor for crosslinking.

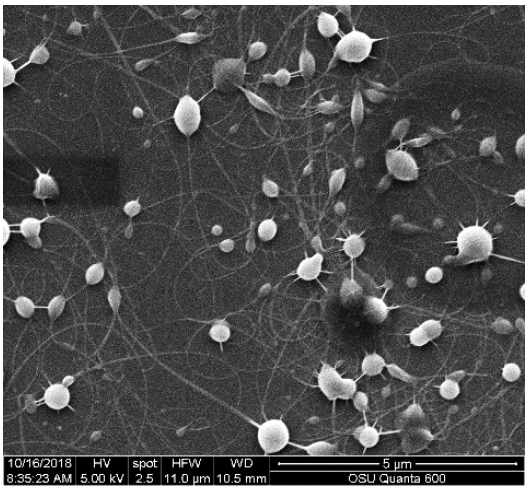

Figure 4.1: Electrospun PVA with GOx on Si coupon from aqueous solvent system.

4.2 Methods

4.2.1 Development of electrospray parameters for glutaraldehyde and glucose oxidase

As a path to go forward, developing PVA/GOx fibers using GA vapor exposure was considered, however it was dismissed since the continuous morphology was less desirable for orientation studies and the technique of electrospinning PVA/GOx fibers and using GA vapor exposure had already been demonstrated by Ren et al. The option of simply incorporating GA and GOx in a solution was then considered for depositing discrete feature morphologies and achieving a stable sensor.

An aqueous preparation of 50 mg/mL glutaraldehyde (GA) and 1 mg/mL glucose oxidase (GOx) was prepared and demonstrated to be readily applicable as an electrospray solution. Shown in Fig. 4.2 – the left image is the Taylor cone behavior during electrospray of the solution (in this case a pulsed high voltage waveform is applied). Stable Taylor cone behavior was observed, meaning there was little variation in the shape of the cone during the electrospray deposition. Shown in the right image of Fig. 4.2 is deposition of the

GA/GOx particles. Electrochemical experiments were carried out using a platinum working electrode prepared by electrospray deposition onto the electrode surface, however this surface was not feasible for imaging. This was due to the platinum electrode being

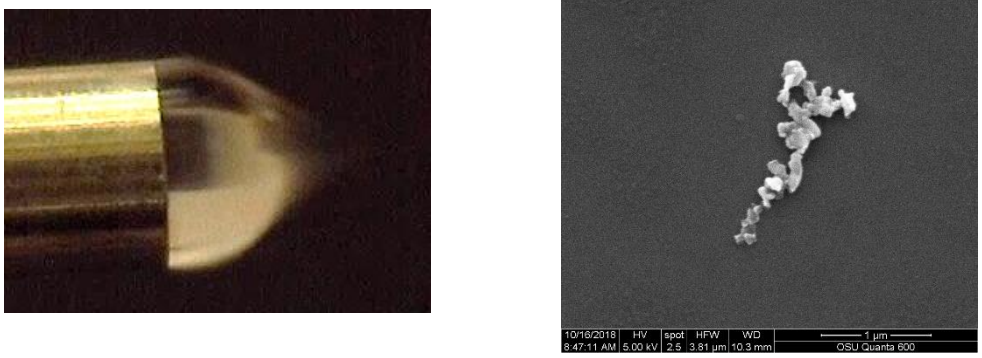

Figure 4.2: (Left) Electrospray deposition of apparent glutaraldehyde/glucose oxidase nanoparticles and stable Taylor cone is achieved. **(Right)** SEM image showing particles collected during electrospray.

mounted on a glass barrel several centimeters in length (making it physically difficult to image in an electron microscope), additionally the electrode could not be sputter-coated without compromising its functionality as an electrochemical sensor. An optical microscope was used to verify that material was indeed deposited on the surface, but the individual morphologies were not visible because the features were too small. Planar silicon wafer chips were used as a substitute substrate to collect images of electrospray deposition. Although, Taylor cone spray behavior is notably different when compared between electrospray onto the two types of substrate, as shown in Fig. 4.3. In this case, the same electrospray parameters were used, the only difference being the type of substrate used as a collector. Thus, the resulting morphology imaged by SEM on the silicon wafer

chip may not be comparable to the morphologies collected by electrospray on the platinum electrode.

Figure 4.3: Electrospray using 40Hz sine wave pulse with 4kVpp and 4kVdc at a 3 cm distance from needle to substrate. **(Left)** Electrospray at a silicon wafer chip substrate. **(Right)** 500µm diameter platinum electrode.

4.2.2 Electrospray methodology

Though the resulting morphologies were not directly observable on the electrode surface, the sensor functionalized by electrospray can still be tested by use electrochemically to verify the presence of active enzyme. With the overall goal being to demonstrate differences in the resulting sensor response between pulsed and DC electrospray depositions, a baseline DC performance was first established. To compare pulsed high voltage waveform depositions to the constant DC deposition, the pulsed signal was set to have a maximum voltage at the constant DC level and a minimum at half the maximum. This was chosen so that no electrospray should occur during the pulse minimum time of the high voltage waveform. During the time that the waveform is at its peak there is the same field strength as the constant DC voltage.

A general working space for electrospray parameters was determined experimentally by starting from parameters established previously for aqueous electrospray solvent systems. We have been successful electrospraying a 10 mg/mL

aqueous solution of polyvinyl alcohol with a 2kV/cm applied field strength, so this was considered as the starting point for electrical parameters. Since enzyme is not storable at room temperature, electrospray was carried out immediately after preparation of the GA/GOx solution. After electrospray, electrodes were either immediately used for electrochemical tests or stored at 4C to minimize any degradation which could impact the sensor performance.

4.3 Results of electrochemical sensor performance

With stable starting parameters for electrospray of the GA/GOx solution, the impact on the sensor response due to variations in these parameters was studied; specifically, the comparison between using DC and pulsed DC for deposition. The most stable sensor performance with a DC deposition was achieved using parameters of 9kVdc applied with a 4cm needle-to-collector distance for 30 second depositions. For this data, the change of current response of the sensor to standard additions of analyte is normalized to the electrode surface area and molarity of target analyte (glucose). Sensors prepared with these DC parameters gave responses of 0.2, 0.3 and 1 $\mu A/cm^2.mM$ (N = 3). The most stable set of sensors functionalized by pulsed deposition used the parameters of a 40Hz sine wave with 4kVpp at a 4kVdc offset over a 3cm needle-to-collector distance for a 30 second deposition. This resulted in normalized responses of 0.5, 1.2 and 3 $\mu A/cm^2.mM$ (N = 3). These results are compared in the graph in Fig. 4.4. There is significant overlap in the range of sensor response between the two electrospray parameters (pulsed vs. DC) and the range of variation of the sensor responses is quite large. Though, it may also be valid to note that

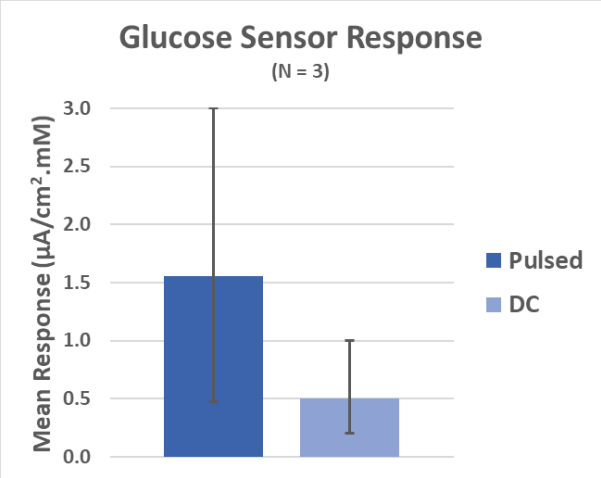

Figure 4.4: Comparison of sensor response between pulsed DC (40Hz sine wave) and DC deposition.

direct comparison of pulsed DC vs DC depositions performed for the same period of time may not be entirely compatible. The pulsed parameters used had a voltage minimum at half that of the peak voltage. This means that the necessary voltage to sustain electrospray was not constantly provided (only for half of the period). The pulsed electrospray deposition should then result in less material being deposited over the same period of time as a constant DC deposition, provided the electrode surface is not already completely saturated during the deposition time.

It must be noted that the magnitude of the response from electrodes prepared using electrospray is much lower than the conventional direct pipetting/drop-casting approach by one-to-two orders of magnitude. In the optimized drop-casting, functionalizing the electrode with a volume of 0.3µL of solution gave a sensitivity of 60 µA/cm^2.mM. It was not considered initially to optimize to comparable volumes to compare between the optimization for electrospray and drop-cast; an electrospray time of 30 seconds was chosen. At a 50 µL/hr flow rate the 30 second deposition means ~0.4 µL of solution could be

electrosprayed. Use of the 30 second deposition was continued, to make comparisons between the electrospray results comparable, but as a result the volume of solution is not comparable to the drop-cast results. Regardless, the drop-cast approach generated much greater signal, so more value was to be found in comparing results between electrospray parameters than comparing them to drop-cast. Because it is also likely that not all electrosprayed material is collected on the electrode surface, comparison of the same volume for drop-cast and electrospray may not be relevant anyway. It is also questionable whether considering time and flow rate alone is enough to determine how much volume of solution has been electrosprayed. Without being able to quantify the amount of material on the electrode, from either preparation method, it is difficult to make comparisons between the two.

There were several parameter sets for both DC and pulsed deposition that did not show stable sensor response. For DC: 8kV at 3cm gave a high magnitude response (5 $\mu A/cm^2$.mM) but had significant signal decay and cannot be considered a reliable response. With pulsed deposition: 40 Hz sine, square and triangle waveforms at 4kVdc and 5kVpp at 4cm distance and 30, 15, and 5 seconds depositions either gave no response or had significant signal decay. Additionally, the sensors which were not stable for use as an electrochemical electrode showed high capacitance, meaning that material was deposited onto the electrode surface but was evidently not active for glucose interaction.

Unfortunately, comparing successful DC and pulsed DC parameters was not achieved using the same deposition distance. A functional sensor was not achieved from DC deposition at 3cm using constant voltage at 8kV (the peak voltage used with pulsed

deposition at 3cm). Likewise, a functional sensor was not achieved from pulsed depositions at the 4cm distance using a peak voltage at 9kV (the constant DC voltage used in depositions at 4cm). So, a comparable parameter set was not achieved for the same deposition distance to allow direct comparisons to be made in that parameter.

Going forward, it would be preferable to develop parameters for pulsed DC and DC depositions which allow comparing deposition at the same distances. The range of pulsed parameters is a large space and making informative conclusions about pulsed depositions requires having as comparable as possible of parameters, so the impact of pulsed DC can be isolated. These results, showing such variability in sensor stability from different electrospray parameters, are evident of the stability having high dependence on the parameters used. It is not clear how exactly the parameters impact the stability in these cases. Active enzyme could be present on the electrode surface, but unable to conduct current to the electrode – so no signal is detectable. Enzyme could have been deposited in a way where its active sites were not accessible to the glucose. It is not possible to conclude the exact impact on the enzyme deposition through pulsed high voltage parameters.

Chapter 5: Conclusion

5.1 Conclusions, observations and paths forward

An outcome of this research is that the materials demonstrated can readily be deposited as discrete morphologies using electrospinning/electrospray and that pulsed DC deposition can be achieved at frequencies in the 100s of Hz ranges. This was achieved with both protein and polymer materials.

Beaded, discrete features are generally considered as a defect in the goal toward continuous fiber electrospinning, yet in this work their use was demonstrated in two direct applications. First, electrospray deposition of fibrinogen (a protein involved in blood coagulation) onto a point-of-care-applicable blood separation device to enhance device performance. Second, deposition of discrete nanoparticles of the enzyme glucose oxidase for an enzymatic, electrochemical glucose sensor. The deposition of protein nanoparticles on the blood separation device showed clear impact on the fluid flow in the separation performance. Though, the hypothesis that the blood separation could be impacted by the fibrinogen coagulation chemistry is not confirmed. More research would be needed to determine if this is possible. It is possible the fibrinogen protein no longer retains its activity because of the electrospray process and exposure to high potentials and harsh solvents. The ability to functionalize surfaces with nanoparticle material is evident from the results and further work with related applications, or others involving functional nanoparticle deposition, is feasible. Regardless of the exact mechanism at work, depositing these types of morphologies did show an improvement in the separative performance on the membrane devices and is beneficial for the application.

The electrospray of the enzyme glucose oxidase clearly showed the ability of an active material to retain its function through electrospray. The electrochemical sensor response for detection of glucose is conclusive evidence that the enzyme still retains function and was able to generate signal with additions of glucose to the electrochemical sensor system. The magnitude of the response is admittedly low in comparison to conventional enzymatic, electrochemical glucose sensor preparation techniques (direct pipetting, drop-cast, of solution); however, it is difficult to determine how efficient electrospraying the enzyme is for functionalizing the sensor surface. It is quite likely that results from the two methods are not directly comparable. By estimation of the amount of material electrosprayed using solution flow rate and elapsed deposition time, a comparable volume was electrosprayed and drop-cast. But, if the entire volume is not deposited on the electrode then the sensor response magnitudes can't be compared directly. There was not a method available to quantify the amount of enzyme deposited using electrospray. Knowing the amount of material deposited is also essential to comparison of pulsed DC vs DC depositions, which is discussed in 5.2.2.

Comparing morphological differences in pulsed DC vs DC deposited features we saw variation in some experiments. The most definitive being the results shown in Chapter 2.3.3, showing a distinction in the size distribution of measured features between samples prepared with pulsed vs non-pulsed. But, the results shown in 2.3.3 also display variability between samples prepared under the same conditions. Additionally, there was variability in how material deposits based on age of solution – Appendix B.1.1. That being said, the results give confidence that deposition behavior can be altered by the use of pulsed high

voltages. Though, the work by no means fully describes the extent to which control can be realized. This area can certainly be investigated further.

An overarching goal in this work was to achieve control of these morphologies, during the deposition process, through the applied electric field. It was hypothesized that a pulsed DC high voltage could impart orientation forces on the particles in-flight. Through the empirical research in this work, that was not realized. In all, this work has provided some outline to a parameter space where deposition of discrete morphologies is achievable. Further work could be pursued to better understand this parameter space and the appropriate ranges for specific materials of interest. To achieve the goal of electrospraying individual species and effecting orientation in flight, there are several factors which likely need to be extensively investigated prior; controlling electrosprayed particle size, quantitatively assessing effective orientation, and molecular dynamics simulation.

5.2 Paths forward

5.2.1 Generation of individual molecules in electrospray

The size of the deposited features seen from protein and polymer materials is consistent with several agglomerated molecules (instead of individual). To be able to impart orientation forces on the dipole of a molecule would likely require generation of single molecules during the electrospray process. If multiple molecules agglomerate, it is likely their dipole is impacted. This could still allow the desired outcome, but if the goal is to orient an individual species, so an active binding site (such as on antibodies or enzymes)

is favorably oriented from a substrate surface, then agglomeration is likely not advantageous.

An aspect which complicates generation of individual molecules was observed in material concentration in the electrospray solution. Electrospray ionization of intact IgG is reported in white papers by Agilent Technologies[82] and Water Corporation[83]. In these reports they dilute intact IgG antibodies to concentrations of 0.1 – 1 mg/mL. Waters reports performing LC/MS on intact IgG from 0.1 – 0.5 mg/mL in 50mM ammonium bicarbonate solutions. The Agilent report specifies solution preparation by dilution of 1 mg/mL IgG into 20% v/v acetonitrile. In our electrospray setup, preparations at these low of concentrations were not successful for generation of a Taylor cone, or apparent electrospray behavior. Increasing concentration of protein in solution allowed for some oscillating/intermittent cone behavior, but not with stability and not to an extent where deposition was evident. They also report use of gradient elution LC/MS which was not feasible in our electrospray setup, though gradient elution primarily functions in a capacity for separations. It is possible that using the solution preparations reported and devising an apparatus setup more similar to the ESI-MS interface would be conducive to generating electrospray. However, in terms of surface functionalization, these concentrations are orders of magnitude lower than typical concentrations used for this research. For example, when electrospraying the 2 mg/mL fibrinogen solutions, observable surface coating was achieved after minutes of the process. So, it is likely that electrospray with such low concentrations of material would require hours per deposition, if electrospray could be generated. If a setup could be devised which reduced, or focused, the deposition area then

this time could likely be reduced. However, attempts to electrospray fibrinogen at 0.1 – 1 mg/mL in this work were unsuccessful due to no stable electrospray being established. It seems that, for the setup and conditions used in this research, the parameter ranges necessary to generate electrospray of individual molecules and generate any electrospray are not in agreement. Identifying how to achieve this would be the first step forward on the path toward electrospray of individual molecules for electrospray deposition and surface functionalization.

5.2.2 Measuring orientation of deposited species

Another critical aspect is the ability to determine the orientation of antibodies deposited on a substrate. One method is atomic force microscopy (AFM) used in conjunction with fluorescent labelled antibodies (FITC tagged), demonstrated for IgG immobilization in a microfluidic device under an applied electric field[84]. This combination allows determination of the consistency in orientation of the antibodies (through the AFM) in relation to each other and combines a fluorescent signal intensity to determine the accessibility of the active site. Difficulty still arises in comparison of pulsed DC deposition to constant DC deposition parameters. If the experiment is conducted so that deposition is performed for the same duration, then the amount of deposited material may not be comparable. If pulsed parameters are set so the magnitude of the minimum pulse value is below the magnitude to cause electrospray, then a pulsed DC deposition for the same duration as a DC will have less active electrospray time. If the signal resulting from the pulsed DC deposition is equal to, or greater than, the DC deposition then it can be

inferred that the pulsed deposition has greater orientation which is leading to the greater signal intensity. It would then be critical to determine the amount of material deposited in each case (pulsed DC and DC depositions) to make quantitative signals from each comparable. Without this ability, it is possible different amounts of material are deposited, which alone could account for the differences in signal intensity.

5.2.3 Computational modeling to focus empirical investigation

To determine pulsed electrical parameter sets to work with, implementation of gas phase molecular dynamics modeling would be beneficial. This is especially true if electrospray deposition of individual (not agglomerated) species requires working with concentrations which would take hours to sufficiently coat a substrate. These deposition times would not be conducive to entirely empirical-based studies. Simulation modeling could help to identify appropriate parameters to focus investigation. Molecular dynamics simulation approaches for studying protein behavior during the ESI process have been demonstrated[85,86]. However, these are computationally intensive algorithms, requiring GPU acceleration and programming, and can only simulate nanosecond to microsecond experiment runs. But, in this case every atom in the electrosprayed protein, and its movement, is simulated for the run time window. Modeling was not implemented during this work, but its use to determine appropriate parameter sets for electrospray of low concentration species is a likely component in a path forward. Experiment design must be thoroughly considered to result in evidence that proves pulsed deposition increases orientation of these species.

Bibliography:

[1] N. Tucker and H. Razzaq, “The History of the Science and Technology of Electrospinning from 1600 to 1995,” *Journal of Engineered Fibers and Fabrics*, p. 11, 2012.
[2] J. Zeleny, “The Electrical Discharge from Liquid Points, and a Hydrostatic Method of Measuring the Electric Intensity at Their Surfaces,” *Physical Review*, vol. 3, no. 2, pp. 69–91, Feb. 1914.
[3] A. Formhals, “Process and Apparatus for Preparing Artificial Threads,” 1,195,504, 02-Oct-1934.
[4] G. Taylor, “Disintegration of water drops in an electric field,” *Proceedings of the Royal Society A*, vol. 280, no. 1382, p. 18, Jul. 1964.
[5] J. Doshi and D. H. Reneker, “Electrospinning Process and Applications of Electrospun Fibers,” *Journal of Electrostatics*, vol. 35, pp. 151–160, 1995.
[6] S. A. Theron, E. Zussman, and A. L. Yarin, “Experimental investigation of the governing parameters in the electrospinning of polymer solutions,” *Polymer*, vol. 45, no. 6, pp. 2017–2030, Mar. 2004.
[7] S. A. Sell, M. J. McClure, K. Garg, P. S. Wolfe, and G. L. Bowlin, “Electrospinning of collagen/biopolymers for regenerative medicine and cardiovascular tissue engineering,” *Advanced Drug Delivery Reviews*, vol. 61, no. 12, pp. 1007–1019, Oct. 2009.
[8] W. Wang *et al.*, “Humidity sensor based on LiCl-doped ZnO electrospun nanofibers,” *Sensors and Actuators B: Chemical*, vol. 141, no. 2, pp. 404–409, Sep. 2009.
[9] C. J. Angammana and S. H. Jayaram, “Fundamentals of electrospinning and processing technologies,” *Particulate Science and Technology*, vol. 34, no. 1, pp. 72–82, Jan. 2016.
[10] C. M. Vaz, S. van Tuijl, C. V. C. Bouten, and F. P. T. Baaijens, “Design of scaffolds for blood vessel tissue engineering using a multi-layering electrospinning technique,” *Acta Biomaterialia*, vol. 1, no. 5, pp. 575–582, Sep. 2005.
[11] J. A. Matthews, G. E. Wnek, D. G. Simpson, and G. L. Bowlin, “Electrospinning of Collagen Nanofibers,” *Biomacromolecules*, vol. 3, no. 2, pp. 232–238, Mar. 2002.
[12] G. E. Wnek, M. E. Carr, D. G. Simpson, and G. L. Bowlin, “Electrospinning of Nanofiber Fibrinogen Structures,” *Nano Letters*, vol. 3, no. 2, pp. 213–216, Feb. 2003.
[13] S. J. Eichhorn and W. W. Sampson, “Relationships between specific surface area and pore size in electrospun polymer fibre networks,” *J. R. Soc. Interface*, vol. 7, no. 45, pp. 641–649, Apr. 2010.
[14] R. Gopal, S. Kaur, Z. Ma, C. Chan, S. Ramakrishna, and T. Matsuura, “Electrospun nanofibrous filtration membrane,” *Journal of Membrane Science*, vol. 281, no. 1–2, pp. 581–586, Sep. 2006.
[15] S. S. A. An and Rajangam, “Fibrinogen and fibrin based micro and nano scaffolds incorporated with drugs, proteins, cells and genes for therapeutic biomedical applications,” *International Journal of Nanomedicine*, p. 3641, Sep. 2013.

[16] E. Chong *et al.*, "Evaluation of electrospun PCL/gelatin nanofibrous scaffold for wound healing and layered dermal reconstitution☆," *Acta Biomaterialia*, vol. 3, no. 3, pp. 321–330, May 2007.
[17] G. Zhao, B. Huang, J. Zhang, A. Wang, K. Ren, and Z. L. Wang, "Electrospun Poly(L -Lactic Acid) Nanofibers for Nanogenerator and Diagnostic Sensor Applications," *Macromolecular Materials and Engineering*, vol. 302, no. 5, p. 1600476, May 2017.
[18] D. Li, M. W. Frey, and A. J. Baeumner, "Electrospun polylactic acid nanofiber membranes as substrates for biosensor assemblies," *Journal of Membrane Science*, vol. 279, no. 1–2, pp. 354–363, Aug. 2006.
[19] L. M. Shepherd, E. González, E. X. Chen, and M. W. Frey, "Increasing Stability of Biotin Functionalized Electrospun Fibers for Biosensor Applications," *ACS Applied Materials & Interfaces*, vol. 9, no. 2, pp. 1968–1974, Jan. 2017.
[20] K. B. Paul, V. Singh, S. R. K. Vanjari, and S. G. Singh, "One step biofunctionalized electrospun multiwalled carbon nanotubes embedded zinc oxide nanowire interface for highly sensitive detection of carcinoma antigen-125," *Biosensors and Bioelectronics*, vol. 88, pp. 144–152, Feb. 2017.
[21] E. González, L. Shepherd, L. Saunders, and M. Frey, "Surface Functional Poly(lactic Acid) Electrospun Nanofibers for Biosensor Applications," *Materials*, vol. 9, no. 1, p. 47, Jan. 2016.
[22] X. Song, Q. Qi, T. Zhang, and C. Wang, "A humidity sensor based on KCl-doped SnO2 nanofibers," *Sensors and Actuators B: Chemical*, vol. 138, no. 1, pp. 368–373, Apr. 2009.
[23] B. Wang *et al.*, "A novel route to prepare $LaNiO_3$ perovskite-type oxide nanofibers by electrospinning for glucose and hydrogen peroxide sensing," *Analyst*, vol. 138, no. 1, pp. 362–367, 2013.
[24] Z. Zhang, S. Gu, Y. Ding, J. Jin, and F. Zhang, "Determination of l-tryptophane using a sensor platform based on LaCoO3 poriferous nanofibers by electrospinning," *Anal. Methods*, vol. 5, no. 18, p. 4859, 2013.
[25] M. Zhi, A. Koneru, F. Yang, A. Manivannan, J. Li, and N. Wu, "Electrospun $La_{0.8}Sr_{0.2}MnO_3$ nanofibers for a high-temperature electrochemical carbon monoxide sensor," *Nanotechnology*, vol. 23, no. 30, p. 305501, Aug. 2012.
[26] X. Yue, T. Hong, Z. Yang, and S. Huang, "Room temperature H2S micro-sensors with anti-humidity properties fabricated from NiO-In2O3 composite nanofibers," *Chin. Sci. Bull.*, vol. 58, no. 7, pp. 821–826, Mar. 2013.
[27] L. Almany and D. Seliktar, "Biosynthetic hydrogel scaffolds made from fibrinogen and polyethylene glycol for 3D cell cultures," *Biomaterials*, vol. 26, no. 15, pp. 2467–2477, May 2005.
[28] R. M. D. Soares, N. M. Siqueira, M. P. Prabhakaram, and S. Ramakrishna, "Electrospinning and electrospray of bio-based and natural polymers for biomaterials development," *Materials Science and Engineering: C*, vol. 92, pp. 969–982, Nov. 2018.
[29] M. C. McManus, E. D. Boland, D. G. Simpson, C. P. Barnes, and G. L. Bowlin, "Electrospun fibrinogen: Feasibility as a tissue engineering scaffold in a rat cell

culture model," *Journal of Biomedical Materials Research Part A*, vol. 81A, no. 2, pp. 299–309, May 2007.
[30] S. A. Sell, P. S. Wolfe, K. Garg, J. M. McCool, I. A. Rodriguez, and G. L. Bowlin, "The Use of Natural Polymers in Tissue Engineering: A Focus on Electrospun Extracellular Matrix Analogues," *Polymers*, vol. 2, no. 4, pp. 522–553, Nov. 2010.
[31] "Elmarco Nanospider Production Lines," *Elmarco*. [Online]. Available: https://elmarco.com/production-lines. [Accessed: 18-May-2019].
[32] "Bioinicia laboratory equipment," *Bioinicia*. [Online]. Available: https://bioinicia.com/electrospinning-electrospraying-lab-equipment/. [Accessed: 18-May-2019].
[33] "inovenso laboratory electrospinning equipment," *inovenso*. [Online]. Available: https://www.inovenso.com/product/laboratory-electrospinning-equipments/. [Accessed: 18-May-2019].
[34] "Linari electrospinning equipment," *Linari nanotech*. [Online]. Available: http://www.linaribiomedical.com/index.php/electrospinning/electrospinning-equipments. [Accessed: 18-May-2019].
[35] "Yflow electrospinning equipment," *Yflow*. [Online]. Available: http://www.yflow.com/electrospinning-machine/. [Accessed: 18-May-2019].
[36] C. Yang, Z. Jia, Z. Xu, K. Wang, Z. Guan, and L. Wang, "Comparisons of fibers properties between vertical and horizontal type electrospinning systems," in *2009 IEEE Conference on Electrical Insulation and Dielectric Phenomena*, Virginia Beach, VA, USA, 2009, pp. 204–207.
[37] S. L. Shenoy, W. D. Bates, H. L. Frisch, and G. E. Wnek, "Role of chain entanglements on fiber formation during electrospinning of polymer solutions: good solvent, non-specific polymer–polymer interaction limit," *Polymer*, vol. 46, no. 10, pp. 3372–3384, Apr. 2005.
[38] Z.-C. Xing, J. Yuan, W.-P. Chae, I.-K. Kang, and S.-Y. Kim, "Keratin Nanofibers as a Biomaterial," p. 5.
[39] M. Wilm, "Principles of Electrospray Ionization," p. 8.
[40] L. Konermann, E. Ahadi, A. D. Rodriguez, and S. Vahidi, "Unraveling the Mechanism of Electrospray Ionization," *Anal. Chem.*, vol. 85, no. 1, pp. 2–9, Jan. 2013.
[41] P. Kebarle and U. H. Verkerk, "On the Mechanism of Electrospray Ionization Mass Spectrometry (ESIMS)," in *Electrospray and MALDI Mass Spectrometry*, R. B. Cole, Ed. Hoboken, NJ, USA: John Wiley & Sons, Inc., 2012, pp. 1–48.
[42] J. Dong, A. D. Asandei, and R. S. Parnas, "Aqueous electrospinning of wheat gluten fibers with thiolated additives," *Polymer*, vol. 51, no. 14, pp. 3164–3172, Jun. 2010.
[43] C. J. Angammana and S. H. Jayaram, "Fundamentals of electrospinning and processing technologies," *Particulate Science and Technology*, vol. 34, no. 1, pp. 72–82, Jan. 2016.
[44] Y. M. Shin, M. M. Hohman, M. P. Brenner, and G. C. Rutledge, "Experimental characterization of electrospinning: the electrically forced jet and instabilities," *Polymer*, vol. 42, no. 25, pp. 09955–09967, Dec. 2001.

[45] H. Fong, I. Chun, and D. H. Reneker, "Beaded nanofibers formed during electrospinning," *Polymer*, vol. 40, no. 16, pp. 4585–4592, Jul. 1999.
[46] Y. Liu, J.-H. He, J. Yu, and H. Zeng, "Controlling numbers and sizes of beads in electrospun nanofibers," *Polymer International*, vol. 57, no. 4, pp. 632–636, Apr. 2008.
[47] T.-L. Chang, C.-H. Huang, S.-Y. Chou, S.-F. Tseng, and Y.-W. Lee, "Direct fabrication of nanofiber scaffolds in pillar-based microfluidic device by using electrospinning and picosecond laser pulses," *Microelectronic Engineering*, vol. 177, pp. 52–58, Jun. 2017.
[48] J. Pelipenko, J. Kristl, B. Janković, S. Baumgartner, and P. Kocbek, "The impact of relative humidity during electrospinning on the morphology and mechanical properties of nanofibers," *International Journal of Pharmaceutics*, vol. 456, no. 1, pp. 125–134, Nov. 2013.
[49] S. De Vrieze, T. Van Camp, A. Nelvig, B. Hagström, P. Westbroek, and K. De Clerck, "The effect of temperature and humidity on electrospinning," *Journal of Materials Science*, vol. 44, no. 5, pp. 1357–1362, Mar. 2009.
[50] H. Fashandi and M. Karimi, "Pore formation in polystyrene fiber by superimposing temperature and relative humidity of electrospinning atmosphere," *Polymer*, vol. 53, no. 25, pp. 5832–5849, Nov. 2012.
[51] Y. T. Aliyev, B. M. Dabynov, D. U. Bodykov, U. S. Musabekov, and Z. A. Mansurov, "Development and Use of a Modified Pulse Electrospinning Setup for Producing Short Fibers," *Journal of Engineering Physics and Thermophysics*, vol. 89, no. 1, pp. 265–271, Jan. 2016.
[52] Q. Zhang, L. Wang, Z. Wei, X. Wang, S. Long, and J. Yang, "Large-scale aligned fiber mats prepared by salt-induced pulse electrospinning," *Journal of Polymer Science Part B: Polymer Physics*, vol. 50, no. 14, pp. 1004–1012, Jul. 2012.
[53] R. Baba, C. J. Angammana, S. H. Jayaram, and L.-T. Lim, "An IGBT-Based Pulsed Power Supply for Fabricating Noncontinuous Nanofibers Using Electrospinning," *IEEE Transactions on Industry Applications*, vol. 49, no. 4, pp. 1801–1807, Jul. 2013.
[54] S. Köhler, F. Schmid, and G. Settanni, "The Internal Dynamics of Fibrinogen and Its Implications for Coagulation and Adsorption," *PLOS Computational Biology*, vol. 11, no. 9, p. e1004346, Sep. 2015.
[55] S. A. Sell, M. J. McClure, K. Garg, P. S. Wolfe, and G. L. Bowlin, "Electrospinning of collagen/biopolymers for regenerative medicine and cardiovascular tissue engineering," *Advanced Drug Delivery Reviews*, vol. 61, no. 12, pp. 1007–1019, Oct. 2009.
[56] M. C. McManus, E. D. Boland, D. G. Simpson, C. P. Barnes, and G. L. Bowlin, "Electrospun fibrinogen: Feasibility as a tissue engineering scaffold in a rat cell culture model," *Journal of Biomedical Materials Research Part A*, vol. 81A, no. 2, pp. 299–309, May 2007.
[57] N. Laurens, P. Koolwijk, and M. P. M. De Maat, "Fibrin structure and wound healing," *Journal of Thrombosis and Haemostasis*, vol. 4, no. 5, pp. 932–939, May 2006.

[58] "Fibrinogen from bovine plasma." Sigma Aldrich, 2017.
[59] S. A. Smith, R. J. Travers, and J. H. Morrissey, "How it all starts: Initiation of the clotting cascade," *Critical Reviews in Biochemistry and Molecular Biology*, vol. 50, no. 4, pp. 326–336, Jul. 2015.
[60] S. S. Shahrabi, J. Barzin, and P. Shokrollahi, "Blood cell separation by novel PET/PVP blend electrospun membranes," *Polymer Testing*, vol. 66, pp. 94–104, Apr. 2018.
[61] Z. Modrzejewska and W. Eckstein, "Chitosan hollow fiber membranes," *Biopolymers*, vol. 73, no. 1, pp. 61–68, Jan. 2004.
[62] A. Higuchi, S. Yamamiya, B. O. Yoon, M. Sakurai, and M. Hara, "Peripheral blood cell separation through surface-modified polyurethane membranes," *J. Biomed. Mater. Res.*, vol. 68A, no. 1, pp. 34–42, Jan. 2004.
[63] K. A. L. Hector, "Dullaert, Geleen (NL); Marko," 2013/0256230 A1.
[64] J. McDowall, "Fibrinogen," *European Bioinformatics Institute*. [Online]. Available: https://www.ebi.ac.uk/interpro/potm/2006_11/Page1.htm. [Accessed: 05-May-2019].
[65] G. C. Bandara, "Comprehensive, Low-Cost Wicking Microfluidic Analytical Devices for Clinical Diagnostics and Environmental Analysis," Oregon State University, 2019.
[66] A. Lodge, "What's the Difference Between Serum and Plasma?," *Astarte Biologics*. [Online]. Available: https://astartebio.com/blog/ask-scientist-whats-difference-serum-plasma/. [Accessed: 05-May-2019].
[67] "Ethylenediaminetetraacetic acid," *U.S. National Library of Medicine National Center for Biotechnology Information*. [Online]. Available: https://pubchem.ncbi.nlm.nih.gov/compound/edta. [Accessed: 19-Apr-2019].
[68] "Enzymes Function and structure," *Royal Society of Chemistry*. [Online]. Available: https://www.rsc.org/Education/Teachers/Resources/cfb/enzymes.htm. [Accessed: 12-May-2019].
[69] A. K. Trilling, J. Beekwilder, and H. Zuilhof, "Antibody orientation on biosensor surfaces: a minireview," *Analyst*, vol. 138, no. 6, p. 1619, 2013.
[70] F. Cao and J. Gong, "Nonenzymatic glucose sensor based on CuO microfibers composed of CuO nanoparticles," *Analytica Chimica Acta*, vol. 723, pp. 39–44, Apr. 2012.
[71] Y. Liu, H. Teng, H. Hou, and T. You, "Nonenzymatic glucose sensor based on renewable electrospun Ni nanoparticle-loaded carbon nanofiber paste electrode," *Biosensors and Bioelectronics*, vol. 24, no. 11, pp. 3329–3334, Jul. 2009.
[72] A. Tiwari, D. Terada, C. Yoshikawa, and H. Kobayashi, "An enzyme-free highly glucose-specific assay using self-assembled aminobenzene boronic acid upon polyelectrolytes electrospun nanofibers-mat," *Talanta*, vol. 82, no. 5, pp. 1725–1732, Oct. 2010.
[73] R. Hu, J. Wang, P. Chen, Y. Hao, C. Zhang, and X. Li, "Preparation of Cd-Loaded In_2O_3 Hollow Nanofibers by Electrospinning and Improvement of Formaldehyde Sensing Performance," *Journal of Nanomaterials*, vol. 2014, pp. 1–7, 2014.

[74] Q. Lin, Y. Li, and M. Yang, “Polyaniline nanofiber humidity sensor prepared by electrospinning,” *Sensors and Actuators B: Chemical*, vol. 161, no. 1, pp. 967–972, Jan. 2012.
[75] L. Ge, Y. Zhao, T. Mo, J. Li, and P. Li, “Immobilization of glucose oxidase in electrospun nanofibrous membranes for food preservation,” *Food Control*, vol. 26, no. 1, pp. 188–193, Jul. 2012.
[76] G. Ren *et al.*, “Electrospun poly(vinyl alcohol)/glucose oxidase biocomposite membranes for biosensor applications,” *Reactive and Functional Polymers*, vol. 66, no. 12, pp. 1559–1564, Dec. 2006.
[77] X. Su *et al.*, “A New Amperometric Glucose Biosensor Based on One-Step Electrospun PolyVinyl Alcohol-Chitosan Nanofibers,” *Journal of Biomedical Nanotechnology*, vol. 9, pp. 1776–1783, Mar. 2013.
[78] S. Huang, Y. Ding, Y. Liu, L. Su, R. Filosa, and Y. Lei, “Glucose Biosensor Using Glucose Oxidase and Electrospun Mn2O3-Ag Nanofibers,” *Electroanalysis*, vol. 23, no. 8, pp. 1912–1920, Aug. 2011.
[79] J. Wu and F. Yin, “Sensitive enzymatic glucose biosensor fabricated by electrospinning composite nanofibers and electrodepositing Prussian blue film,” *Journal of Electroanalytical Chemistry*, vol. 694, pp. 1–5, Apr. 2013.
[80] M. Scampicchio, A. Arecchi, N. S. Lawrence, and S. Mannino, “Nylon nanofibrous membrane for mediated glucose biosensing,” *Sensors and Actuators B: Chemical*, vol. 145, no. 1, pp. 394–397, Mar. 2010.
[81] J. Manuel *et al.*, “Functionalized polyacrylonitrile nanofibrous membranes for covalent immobilization of glucose oxidase,” *Journal of Biomedical Nanotechnology*, vol. 11, pp. 143–149, 2015.
[82] L. Chen, A. Gieschen, and G. W. Kilby, “Antibody Analysis by ESI-TOF LC/MS,” *Agilent Technologies*, p. 12.
[83] A. Chakraborty, S. Berger, and J. Gebler, “Characterization of an IgG1 Monoclonal Antibody and Related Sub-Structures by LC/ESI-TOF MS,” *Waters*, p. 15.
[84] S. Emaminejad, M. Javanmard, C. Gupta, S. Chang, R. W. Davis, and R. T. Howe, “Tunable control of antibody immobilization using electric field,” *Proc Natl Acad Sci USA*, vol. 112, no. 7, pp. 1995–1999, Feb. 2015.
[85] D. Kim, N. Wagner, K. Wooding, D. E. Clemmer, and D. H. Russell, “Ions from Solution to the Gas Phase: A Molecular Dynamics Simulation of the Structural Evolution of Substance P during Desolvation of Charged Nanodroplets Generated by Electrospray Ionization,” *J. Am. Chem. Soc.*, vol. 139, no. 8, pp. 2981–2988, Mar. 2017.
[86] L. Konermann, H. Metwally, R. G. McAllister, and V. Popa, “How to run molecular dynamics simulations on electrospray droplets and gas phase proteins: Basic guidelines and selected applications,” *Methods*, vol. 144, pp. 104–112, Jul. 2018.

APPENDICES

Appendix A: Transformer-based pulsed system and characterizations

A.1 Transformer system output voltage response characterization

In Table A.1 contains data from characterization of the transformer system in its last iteration. This used a “Steinville” high voltage transformer in place of the Webster/Xerox transformer originally in the first iterations of the system. It also has the brand label “Well” and it is not clear on the exact branding or the manufacturer. The characterization in Table A.1 was done to determine input parameters needed for maintaining a 6kV peak to peak output set to oscillate about 0V. The 6kV voltage was chosen because most electrospray in this work was done in the 5kV magnitude range. The RMS voltage at this frequency was also recorded. This characterization showed the greatest efficiency (output voltage to input voltage) in the 400-600Hz range. Going up in frequency from this range required greater input voltages to achieve the 6kVpp. Around 1kHz it became impossible to maintain the 6kVpp output voltage due to increased input voltage no longer giving an increased output.

Table A.1: Characterizing Steinville/Well transformer in the high voltage transformers system. Data recorded Dec. 21, 2017.

Frequency *(Hz)*	**Input** (Vpp) *(mV)*	**Output** (Vpp centered 0V) *(kV)*	**Vmin** *(kV)*	**Vrms** *(kV)*
60	360	5.96	-2.96	1.88
100	312	6.04	-2.96	1.88
120	312-320	6.04	-3.00	1.92
200	332-340	6.00	-3.00	2.28
300	280-284	5.96	-2.96	2.12
400	204-220	6.00-6.04	-3.00	2.08
500	144-160	6.00	-3.00	2.08-2.12
600	178-190	6.04	-3.04	2.16
700	312-324	5.96-6.00	-3.00 – -2.96	2.12
800	504-508	6.00	-3.00	2.08
900	724	6.00	-2.96	2.08
1000	1200	5.20	-2.56	1.08
1100	1100	4	-2	1.4
1500	1100	1.9	-0.92	0.64

In Table A.2 is data from characterization of the same high voltage transformer system but testing variation in peak-to-peak voltage recorded to maintain a 5kVrms output voltage. Peak-to-peak voltage is seen to start with high magnitudes at lower frequencies and decrease with increase of input frequency. The minimum voltage at the output also shows steady increase with increased frequency. As with the Webster/Xerox transformer, it is not possible to maintain the same voltage parameters between frequencies. This test was done with a load of 40 Giga-ohms on the system. It is not clear what is the impedance of the electrospray system. Representation of the air-gap is likely represented appropriately as very high impedance.

Table A.2: 40GOhm load on Well transformer setup in high voltage pulse system. Recorded Jan. 22, 2018.

Frequency *(Hz)*	**Input** (Vpp) *(mV)*	**Output** (Vpp) *(kV)*	**Vrms** *(kV)*	**Vmin** *(kV)*
120	536	9.7	5.04	0.56
200	472	7.04	5.04	1.52
300	392	5.84	5.04	2.24
400	264	5.04	5.04	2.80
500	188	4.32	5.04	3.12
600	276	3.92	5.04	3.52
700	456	3.44	5.04	3.52
800	680	2.96	5.04	3.84
900	1180	2.48	4.48	3.44

In Table A.3 is data from the same range of input parameters used for the characterization data in Table A.2. In this case, no load was applied on the system. This is a more likely representation of the "load" of an air-gap with electrospray. This data was collected as a comparison between a known load impedance and no load, to contrast the system's output voltage parameters between the two cases. Generally, a lower peak-to-peak voltage was recorded at a given frequency when maintaining the same RMS voltage output as with the load test. However, the same RMS output was not maintained at all frequencies, due to audible static/breakdown sounds from the high voltage portion of the system. In cases where this occurred, the 5kVrms output voltage was not pushed and a lower voltage was used.

Table A.3: No load on high voltage pulse system. Recorded Jan. 22, 2018.

Frequency *(Hz)*	**Input** (Vpp) *(mV)*	**Output** (Vpp) *(kV)*	**Vrms** *(kV)*	**Vmin** *(kV)*
120	536	9.5	4.68	0.72
200	472	6.80	5.12	1.68
300	392	5.76	5.12	2.40
400	264	4.80	4.88	2.80
500	188	4.08	5.04	3.20
600	276	3.68	5.04	3.60
700	456	3.12	4.96	3.68
800	680	2.88	4.96	3.84
900	1180	2.40	4.40	3.52

A.2 Schematic of transformer-based pulse system

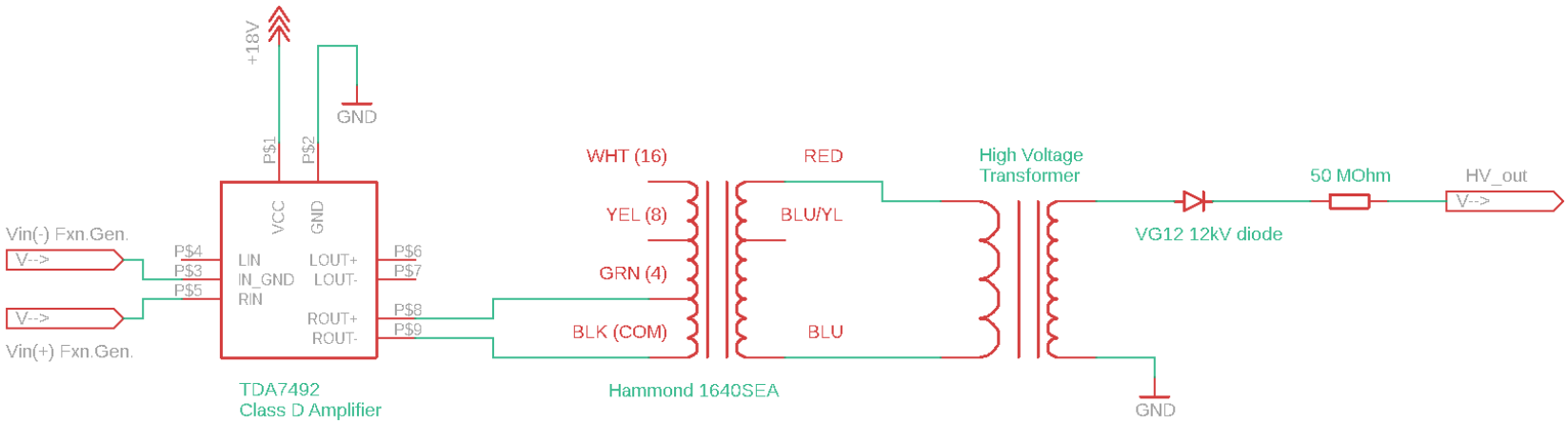

Figure A.1: Schematic of transformer-based pulse system using Well/Steinville high voltage transformer.

Appendix B: Electrospray deposition observations

B.1 Electrospray comparison of pulsed DC to DC

Data presented here in B.1 is based on low number of sample replicates (N=2) and thus were not included in the main text and can only be considered as observations, not conclusions.

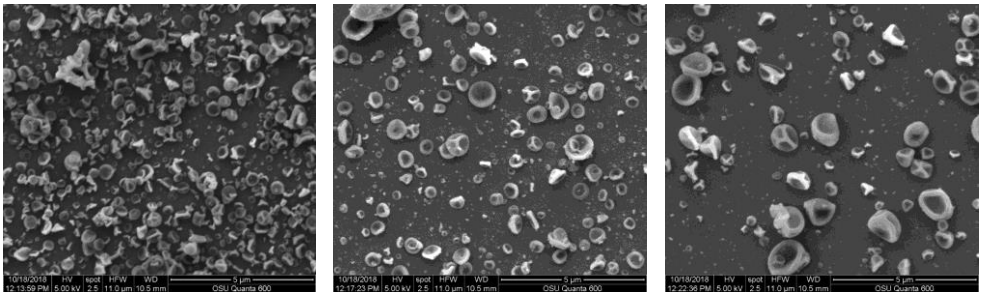

Figure B.1: Electrospun 10 mg/mL wt. fibrinogen on Si coupons. Scale bars 5um **(Left)** ES at DC **(Middle)** ES at 100Hz **(Right)** ES at 500Hz

As in section 2.3.3 in the main text, the SEM images shown in Figure B.1 are from electrospray of fibrinogen comparing DC to pulsed DC deposition. These depositions were performed with the same conditions as there: DC (6kVdc) and 50% duty cycle square wave pulsed DC (3kVpp at 3kVdc offset). There is a notable difference in the results generated at the 500 Hz pulse rate. Large morphologies of nanoparticles are more immediately observable. The size distribution plot in Fig B.2 shows the comparison between the voltage parameters used. The mean in each size bin is determined from multiple images on each substrate and the range in error from between substrates. There is more significant variability in the amount of smaller feature sizes between samples deposited with pulsed depositions than at DC. The size distribution from DC has less significant deviation and a

slight shift to higher feature sizes. These results show some consistency with the results shown from a higher replicate experiment in the main text of this work (Chapter 2.3.3).

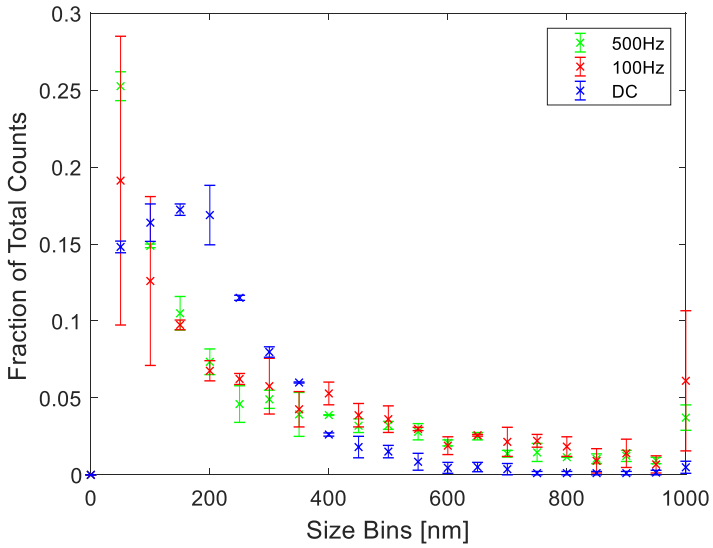

Figure B.2: Size distribution of electrospun fibrinogen at DC, 100Hz and 500Hz parameters. Size bins are 50nm in width.

There is also notable difference between the electrical parameters in the physically observable phenomena during the deposition for these samples, shown in the video screenshot images in Fig. B.3 of Taylor cones during deposition. Deposition at DC shows a typical sharp defined Taylor cone. At 100 Hz pulsed waveform a distinct round aspect of the droplet and concavity in the region of the cone protrusion are observed. The cone tip is

Figure B.3: Electrospun 1% wt. fibrinogen. Scale bars 5um **(Left)** ES at DC **(Middle)** ES at 100Hz **(Right)** ES at 500Hz

less sharp and defined than at DC, but it is still more distinct than at 500 Hz. At the 500 Hz pulse rate the sharp definition of the cone is lost and a broad cone-like protrusion is seen.

B.1.1 Solution age effect on deposition behavior

Duration of time the fibrinogen spends in the prepared solution, after dilution from the stock solution into the organic solvent system, has an apparent effect on the resulting deposited morphology as shown in B.4 with depositions over a several week period. Deposition on the same day as the dilution into the HFP has a noticeably different morphology than the results from electrospraying the same solution after several weeks in solution in HFP. After several weeks, the resulting morphology takes on the cupped shape.

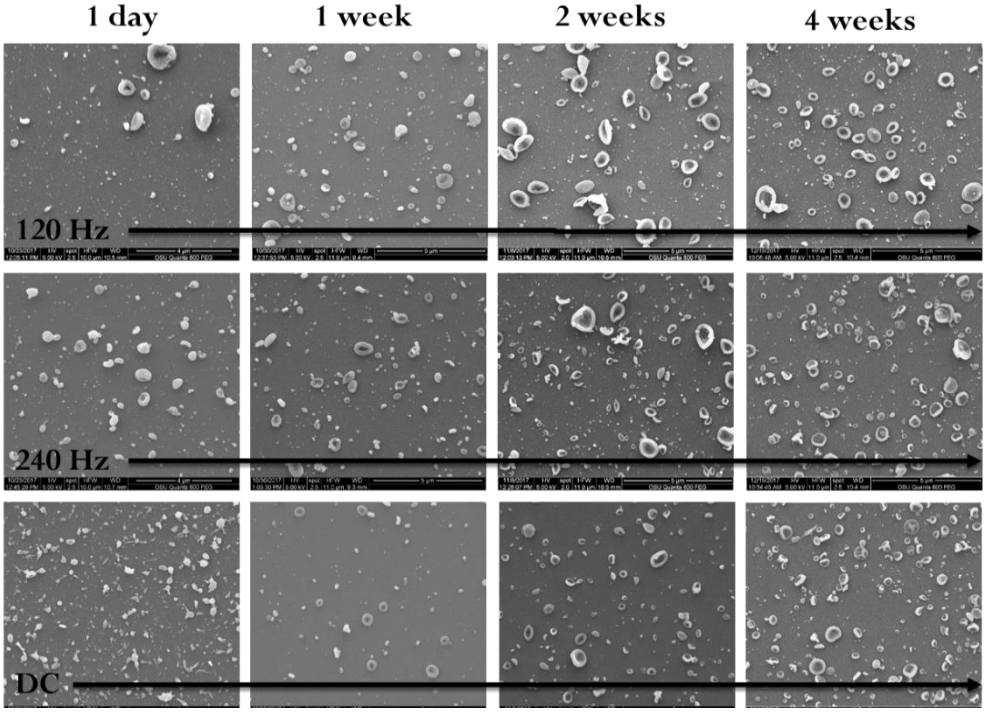

Figure B.4: Electrospun 10 mg/mL fibrinogen. Comparison between DC, 120Hz and 240Hz deposited at time intervals from initial preparation in HFP solution. Scale bars 5um

This made direct comparison between results obtained from the same solution preparation at different points in time possibly inconclusive. To make comparisons, results were considered between parameters compared in deposition on the same day to avoid factors that could not be accounted for. Typically, samples from the same solution, with different parameters, were prepared sequentially.

B.2 Percent counts in feature sizes from experiment in Chapter 2, section 2.3.3.

Table B.1: Percent of feature sizes in measured in each size range. From experiment discussed in Chapter 2, section 2.3.3.

Size Bin (nm)	0-50	50-100	100-150	150-200	200-250	250-300	300-350	350-400	400-450	450-500	500-550	550-600	600-650	650-700	700-750	750-800	800-850	850-900	900-950	950-1000
500HzS1	3.3	54.9	17.7	6.3	2.5	3.1	1.7	1.9	1.9	0.8	***0.4***	***1.0***	***1.0***	***1.5***	***0.4***	***0.4***	***0.6***	***0.2***	***0.2***	***0.0***
500HzS2	5.1	57.5	16.6	5.2	3.1	1.8	1.1	1.7	1.8	2.0	***0.6***	***0.6***	***0.7***	***0.7***	***0.4***	***0.4***	***0.0***	***0.1***	***0.0***	***0.1***
500HzS3	4.8	58.8	17.3	5.3	1.7	2.6	2.0	0.6	1.5	2.2	***0.9***	***0.4***	***0.4***	***0.4***	***0.4***	***0.4***	***0.4***	***0.2***	***0.0***	***0.0***
500HzS4	6.9	63.5	15.7	4.2	2.2	1.1	0.7	1.3	1.0	0.6	***0.7***	***0.8***	***0.1***	***0.3***	***0.4***	***0.4***	***0.0***	***0.1***	***0.0***	***0.0***
500HzS5	5.9	61.0	19.2	3.0	2.3	2.3	0.5	1.6	0.7	0.5	***0.0***	***0.5***	***0.5***	***0.5***	***0.2***	***0.0***	***0.2***	***0.0***	***0.5***	***0.5***
100HzS1	2.9	57.8	17.0	5.2	3.6	3.6	2.3	1.6	1.3	1.5	***1.0***	***0.3***	***0.5***	***0.3***	***0.3***	***0.3***	***0.2***	***0.0***	***0.2***	***0.0***
100HzS2	4.6	58.7	18.1	6.0	3.4	1.4	2.2	0.7	1.7	0.6	***0.4***	***0.1***	***0.6***	***0.1***	***0.6***	***0.4***	***0.0***	***0.3***	***0.0***	***0.0***

100HzS3	3.9	63.2	16.9	4.8	3.2	2.0	1.7	0.9	0.7	0.3	***0.8***	***0.3***	***0.0***	***0.5***	***0.1***	***0.1***	***0.0***	***0.3***	***0.3***	***0.0***
100HzS4	3.4	56.8	18.5	4.4	3.4	2.6	2.1	1.5	2.3	1.1	***1.3***	***0.5***	***0.6***	***0.3***	***0.5***	***0.5***	***0.0***	***0.2***	***0.2***	***0.0***
100HzS5	4.3	61.6	15.1	4.3	3.0	1.7	2.8	1.9	1.9	0.9	***0.9***	***0.3***	***0.4***	***0.1***	***0.1***	***0.0***	***0.4***	***0.0***	***0.0***	***0.1***
DCS1	4.0	58.9	22.6	6.8	3.4	1.9	0.8	0.7	0.3	0.2	***0.1***	***0.0***	***0.0***	***0.0***	***0.0***	***0.0***	***0.0***	***0.0***	***0.0***	***0.0***
DCS2	1.4	30.5	23.6	18.2	9.7	5.9	4.0	2.3	1.6	1.2	***0.7***	***0.5***	***0.1***	***0.1***	***0.0***	***0.1***	***0.0***	***0.1***	***0.0***	***0.0***
DCS3	0.9	26.9	27.7	16.9	10.8	6.0	3.1	3.0	1.8	1.4	***0.6***	***0.2***	***0.2***	***0.2***	***0.2***	***0.1***	***0.0***	***0.0***	***0.0***	***0.0***
DCS4	1.3	26.9	27.6	19.3	11.1	5.5	3.7	2.4	1.0	0.7	***0.3***	***0.1***	***0.1***	***0.0***	***0.0***	***0.0***	***0.0***	***0.0***	***0.0***	***0.0***
DCS5	1.5	31.7	25.4	16.7	10.7	5.8	3.6	2.4	1.0	0.8	***0.4***	***0.1***	***0.0***	***0.0***	***0.0***	***0.1***	***0.0***	***0.0***	***0.0***	***0.0***

B.3 Electrospray solvent system

The results of electrospraying a material can vary based on the solvent system used. Shown here in Figure B.5 is electrospray of Capa 6800 PCL at a 10mg/mL concentration. This is the same concentration and molecular weight of the polymer shown in the images in Chapter 1 Section 1.6.5, Figure 1.5. In that case, continuous or continuous/beaded fibers were seen. Here much more beading is seen. The chloroform solvent was difficult to work with, due to rapid evaporation. It's possible this aspect is what impact the morphology of the deposition.

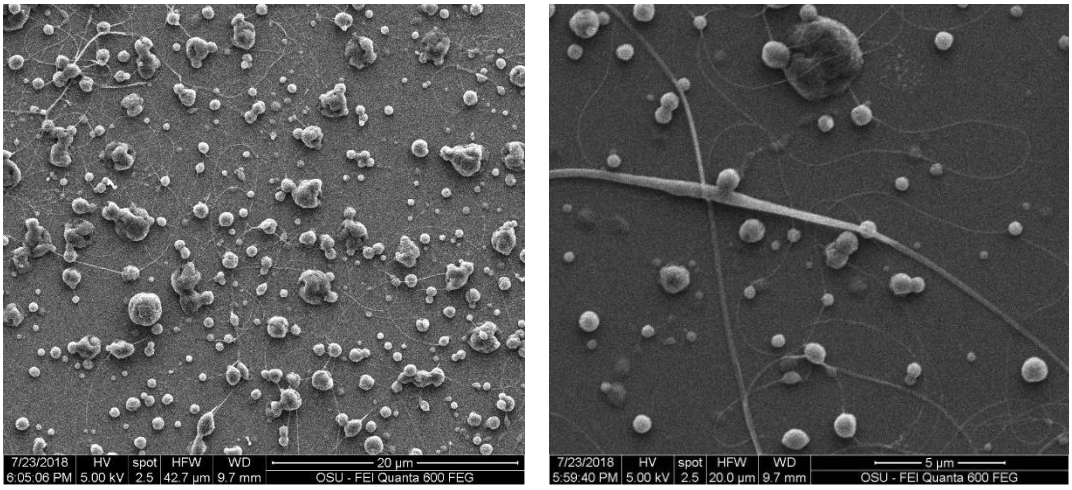

Figure B.5: Electrospun PCL on Si coupon from chloroform solvent system. (Scale **Left** is 20 µm, **Right** is 5 µm)

Appendix C: Supplementary report of electrospray into vacuum chamber

C.1 Introduction

The use of low-vacuum was considered during this work toward controlling orientation on electrosprayed discrete particles. The goal being to use a reduced pressure environment to help eliminate the collisions of the electrosprayed material with gas particles encountered in an ambient pressure setup. A vacuum chamber was purchased from Sanatron, LLC (Salt Lake City, Utah, USA) with modifications made to the door panels to allow electrical connection and solution delivery into the chamber. However, generation of stable electrospray into the vacuum chamber apparatus was not realized in this work. The setup was modified through several iterations to attempt to address issues that were likely impacting the stability of the spray performance. They will be described in more detail in the sections of this appendix. In the first implementation the spray source was located inside the vacuum chamber but saw difficulties with coronal discharge and gas bubble formation in the syringe body. The spray source was relocated outside the chamber and interfaced (by placing in close proximity) to a reduced diameter inlet opening. At first, a metal inlet was used, but a plastic replacement was introduced later due to issues likely to do with the conductively of the metal inlet.

C.2 Electrospray source located inside the chamber

C.2.1 Observation of coronal/plasma discharge

When the spray source was located inside the chamber one of the primary issues encountered was generation of a plasma/corona discharge between the spray needle tip and the collector substrate/counter-electrode when attempting electrospray with a reduced

pressure in the chamber. With the pump running continuously, a pressure difference of -95kPa (relative to ambient) could be reached (or ~40 Torr absolute). A typical field strength used for ambient pressure work was 2kV/cm which was used as a starting point for electrospray in vacuum. However, when attempting to apply high voltages for electrospray, the power supply could not source enough current and the output voltage would drop. At this point, with current greater than 100uA being sourced, a distinct corona discharge around the tip of the needle was visible. With this behavior it wasn't possible to apply a sufficient voltage to cause electrospray. The voltage output could never be increased above 4kV and Taylor cone formation was not observed by locating the collector at an appropriate distance to give the necessary field strength.

C.2.2 Gas bubble formation in solution

An additional issue seen with locating the spray needle inside the chamber was that a large difference in pressure was created across the fluid in the syringe. With this setup, the fluid contained in the syringe experienced an ambient external pressure (around the syringe body and at the syringe's plunger seal) and a low pressure at the needle tip inside the chamber. Using a typical, disposable syringe with a rubber plunger was not possible, because the relative high ambient pressure was too great for the rubber plunger and caused the fluid to be rapidly dispensed from the needle tip, once pressure was reduced in the chamber. Using a disposable syringe with a hard-plastic plunger, or specific gas-tight syringe allowed for more stable fluid pumping. However, after making the interface between the fluid and ambient air more impermeable, it was apparent that dissolved gas in

the fluid was also an issue. While pumping down the chamber to reduced pressures gas bubbles would form in the fluid in the syringe body. During dispensing these bubbles would interrupt the stable flow of the fluid from the needle tip and make electrospray behavior unstable. Bubble formation could be addressed partially by first degassing the solution before loading into the syringe. This was done by placing the fluid in a lidless container inside another vacuum chamber at pressure below 1 Torr (0.7 Torr). Although, with use of a gas-tight syringe and degassing, a corona discharge was still readily formed and no cone behavior was observed.

C.3 Electrospray source located external to vacuum chamber

C.3.1 Metal inlet in chamber feedthrough

The setup was modified so that the entire needle and syringe assembly could be located outside of the vacuum chamber. The needle tip was aligned co-axially with a metal inlet into the chamber. The piece used for this inlet was a 1/4” male-NPT to 1/16” press-fit tubing which threaded into the 1/4" female-NPT vacuum chamber door feedthrough. The needle tip could be located 2-4mm away from the tip of the chamber inlet. With this setup a vacuum pressure of -80kPa could be achieved with the pump running continuously. With no vacuum pressure difference in the chamber, very unstable cone behavior was seen and

was highly intermittent, mostly existing as visually large droplet spray which is shown in Figure C.1.

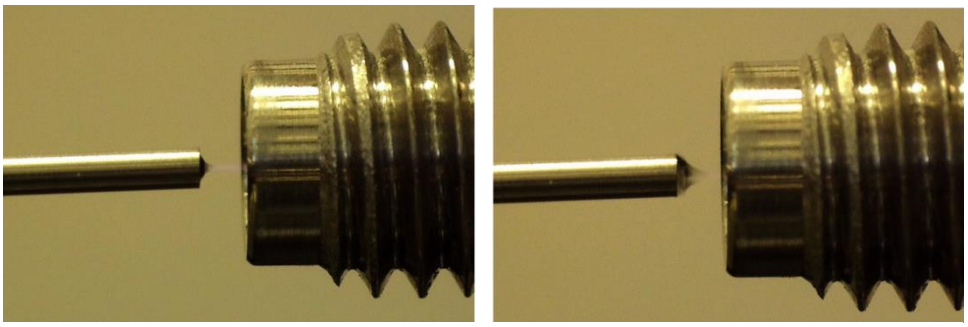

Figure C.1: Electrospray attempted into vacuum chamber with metal inlet/orifice from atmosphere outside (needle side). Pressure in chamber also at ambient. Cone/spray behavior visible but highly infrequent.

This was seen at typical field strengths of 2kV/cm. When a vacuum pressure difference was applied to the chamber a corona/plasma stream was immediately observed. If a droplet was present on the tip of the needle, a strong plasma "beam" was evident, aligned co-axially into the metal inlet. The droplet depleted (likely by evaporation) and finer plasma "strands" were seen connecting between the needle tip and the outer rim of the inlet. In these experiments a wire stub was used as counter-electrode/collector. When the fine plasma was seen connecting the needle tip to the metal inlet, similar strands could also be seen connecting the inlet to the wire sub counter-electrode inside the chamber. This behavior is shown in Figure C.2.

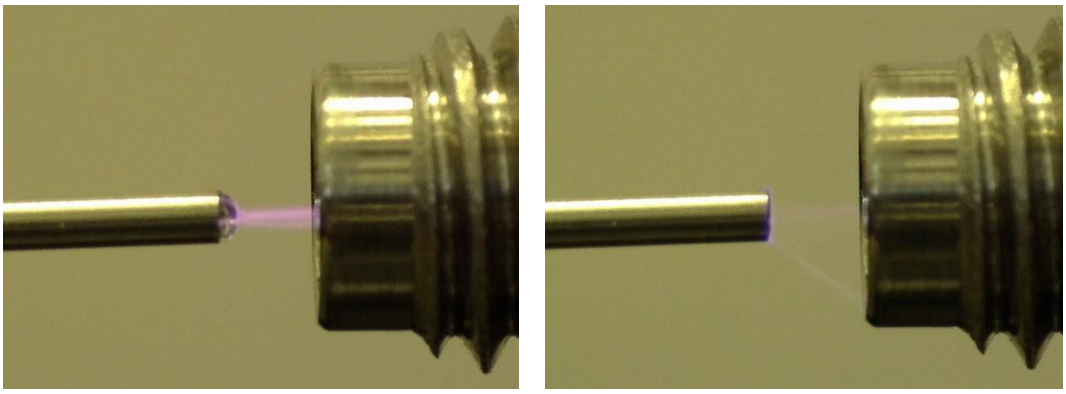

Figure C.2: Electrospray attempted into vacuum chamber with metal inlet/orifice from atmosphere outside (needle side). Vacuum pressure difference of -80kPa from ambient.

C.3.2 Plastic feedthrough inlet

The setup was further modified to use a non-conductive plastic inlet. This piece was created from a pipette tip and glued into a 1/4" male-NPT to 1/8” female-NPT adapter, which threaded into the 1/4" female-NPT chamber door feedthrough. Like the metal inlet, this setup placed a narrow cone tip opening outside the vacuum chamber and allowed the syringe needle spray tip to be located close to the opening. Behavior seen during electrospray is shown in Figure C.3. In Figure C.4 the entire setup is shown, with a cut-away image showing the needle to plastic inlet interface.

With no vacuum pressure difference in the chamber, cone behavior was observed initially after applying the voltage. Cone shape was a broad, not sharp, tip. This progressed into pulsing multi-lobed spray behavior and collection of droplets was evident on the inner surface of the inlet tip. With -90kPa vacuum pressure, a cone formed and was initially oriented into the inlet. However, the cone tip reoriented so that spray was not into the inlet.

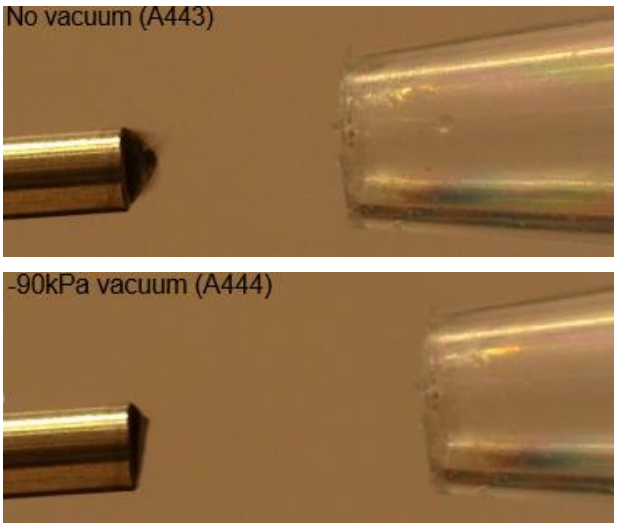

Figure C.3: Electrospray into vacuum chamber with modification of plastic inlet. **(Left)** No vacuum applied with electrospray. Variable cone behavior. Shown here is multi-lobed cones. **(Right)** Electrospray with vacuum pressure difference in chamber. Initially stable behavior, which transitioned to the off-center spray shown.

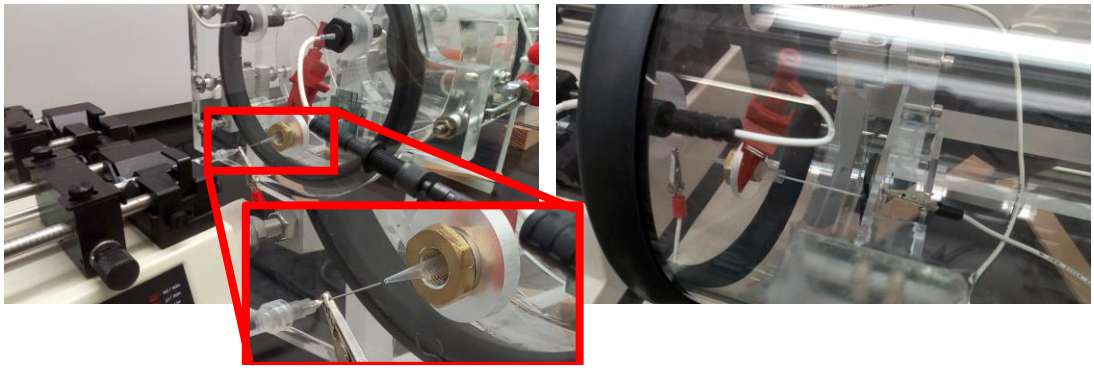

Figure C.4: Final implementation to the vacuum chamber setup. Shown with plastic inlet to chamber. Wire stub collector/counter-electrode used. Metal vacuum feedthrough in door panel was grounded.